Noncontact Atomic Force Microscopy for Atomic-Scale Characterization of Material Surfaces

8

Mehmet Z. Baykara

Contents

Abstract

Among the large variety of scanning probe microscopy techniques, noncontact atomic force microscopy (NC-AFM) stands out with its capability of atomic-resolution imaging and spectroscopy measurements on conducting, semiconducting as well as insulating sample surfaces. In this chapter, we review the fundamental experimental and instrumental methodology associated with the technique and present key results obtained on different classes of material surfaces. In addition to atomic-resolution imaging, the use of NC-AFM towards the goal of atomic-resolution force spectroscopy is emphasized.

Keywords

Atomic Force Microscopy • Atomic Force Spectroscopy

M.Z. Baykara (✉)
Department of Mechanical Engineering and UNAM – Institute of Materials Science and Nanotechnology, Bilkent University, Ankara, Turkey
e-mail: mehmet.baykara@bilkent.edu.tr

C.S.S.R. Kumar (ed.), *Surface Science Tools for Nanomaterials Characterization*,
DOI 10.1007/978-3-662-44551-8_8

1 Definition of the Topic

Since its invention in 1994, noncontact atomic force microscopy (NC-AFM) is routinely being used to image a multitude of material surfaces with atomic resolution. In this chapter, we review the fundamental experimental and instrumental methodology associated with the technique, as well as key results obtained on different classes of material surfaces in the last two decades. In addition to atomic-resolution imaging, the use of NC-AFM towards the goal of atomic-resolution force spectroscopy is also emphasized.

2 Overview

Scanning probe microscopy (SPM) techniques based on the detection of various types of interactions experienced by a sharp probe tip in the vicinity of a sample surface have been used with great success towards high-resolution imaging and measurement of various physical properties since the 1980s. Today, with a large number of manifestations tailored towards different applications, atomic force microscopy (AFM) is one of the most widely used SPM techniques in research and industrial laboratories around the world.

Due to the fact that traditional AFM experiments rely on a *light* contact of the probe tip with the sample surface to detect nanometer-scale topographical features, the interactions of the tip apex with the sample surface are averaged over a finite area, preventing true atomic-resolution imaging. In order to obtain true atomic-resolution imaging on a multitude of material surfaces using an AFM-based approach, the method of noncontact atomic force microscopy (NC-AFM) has been developed. The NC-AFM technique, based on the detection of minor changes in the resonance frequency of an oscillating cantilever due to force interactions between the tip apex atoms and the atoms of the sample surface, does not result in the formation of a finite contact so that experiments can be performed using atomically sharp probe tips. Thus, utilizing NC-AFM, it is possible to image material surfaces with true atomic-resolution *without the formation of a contact* provided that sufficiently sharp probe tips are utilized in conjunction with appropriate experimental procedures.

In addition to its capability of atomic-resolution imaging, NC-AFM has also been employed successfully to perform force spectroscopy (i.e., measure the interaction force acting between the probe tip and the sample surface as a function of tip-sample distance) on well-defined atomic sites on a number of relevant surfaces. Combined with its capability of atomic-resolution imaging, the capability of performing atomic-scale force spectroscopy makes NC-AFM a very powerful tool for the physical and chemical characterization of scientifically and technologically relevant material surfaces for diverse fields of research such as catalysis, adhesion and friction, among others.

Here we provide an introduction to the method of noncontact atomic force microscopy, briefly review the associated experimental and instrumental fundamentals, and report key results in atomic-resolution imaging and force spectroscopy

obtained with the method in the past. Being a subject of continuing research and development, NC-AFM will certainly be used towards a number of different scientific goals in the near future. As such, we will conclude the chapter with a brief outlook regarding future perspectives.

3 Introduction

Despite the fact that properties of solids are largely determined by their atomic structure as well as the associated interatomic interactions has been known for a long time, imaging the atomic structure of material surfaces in real space was first made possible by the relatively recent invention of the scanning tunneling microscope (STM) in the early 1980s by G. Binnig and colleagues [1, 2]. Due to its basic operational principle, which essentially relies on the *quantum tunneling* effect involving the flow of electrons over a vacuum gap between the material surface and a sharp metal probe tip in its vicinity, STM has been extensively used since its invention to image a large number of material surfaces with atomic resolution and measure their electronic properties [3]. Even though a new era in surface science has effectively been started with the introduction of the STM method, due to its fundamental working principle, the technique can only be utilized towards the investigation of conducting and semiconducting surfaces. As such, atomic-scale investigation of insulating material surfaces – such as the majority of metal oxides, a large number of which are scientifically and technologically very relevant – has not been realized with STM. Moreover, STM effectively probes the electronic density of states at the Fermi level associated with the material surface under investigation and therefore, a detailed investigation of various interatomic forces acting between the probe tip and the sample surface is not possible using the technique.

In order to overcome the limitations regarding sample conductivity in STM and the inability of the technique to measure interaction forces, an alternative scanning probe microscopy [4] method – atomic force microscopy (AFM) – has been introduced by Binnig and colleagues at Stanford in 1986 [5]. The operation of the traditional AFM method in the so-called contact mode is based on the controlled approach of a sharp probe tip attached to a micro-machined Si, SiO_2 or SiN cantilever [6–9] to the sample surface under investigation and the subsequent formation of a light contact (Fig. 8.1). While the tip apex is *lightly* touching the sample surface, the tip is raster-scanned in a precisely controlled fashion using piezoelectric scanners and topographic maps of the surface are obtained by detecting the deflection of the cantilever in the vertical direction using techniques such as laser beam deflection [10, 11] and interferometry [12, 13]. Using such an approach, nanoscale topographical maps of various kinds of surfaces have been successfully recorded [14, 15]. Additionally, by simultaneously detecting cantilever twisting around the longitudinal axis in addition to the deflection in the vertical direction, lateral forces experienced by the probe tip can be detected [16, 17], leading to a variation of the method known as *friction force microscopy* (FFM) useful for tribology studies performed on the nanoscale [18].

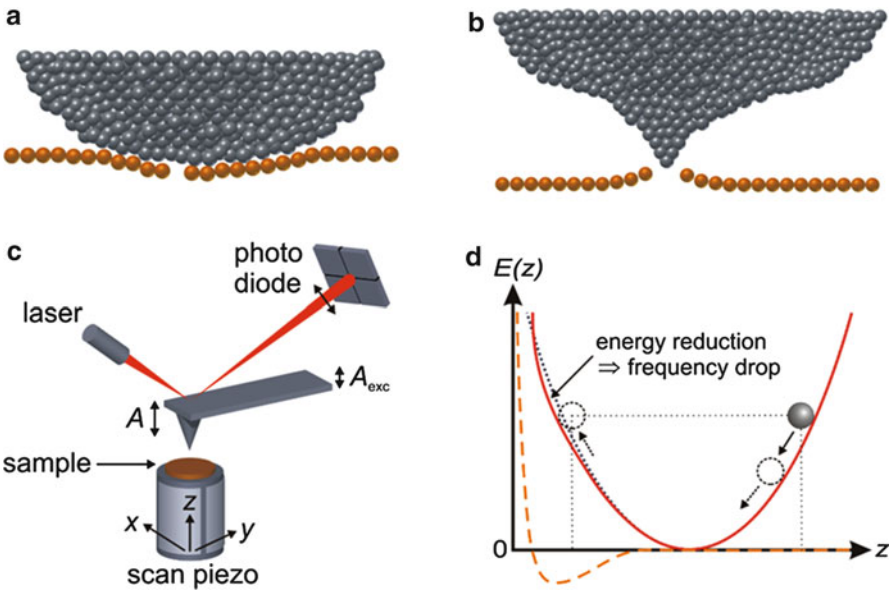

Fig. 8.1 (**a**) Model of an AFM tip in contact with the sample surface. Due to interaction averaging over the finite contact area, the single vacancy is not detected. (**b**) Model of an atomically sharp AFM tip in noncontact operation. Note that the attractive interaction is emphasized by the exaggerated relaxation of the surface around the defect. (**c**) Schematic setup of a typical AFM experiment. During dynamic operation, the cantilever base is excited with an amplitude A_{exc}, leading to an oscillation of the tip with amplitude A. Utilization of a laser source and a photo diode allow detection of cantilever motion whereas the sample is positioned under the tip via a piezoelectric tube (the *scan piezo*). (**d**) The physical origin of the frequency shift during NC-AFM operation is based on the modification of the harmonic oscillation potential of the tip (the *dotted blue line*) due to tip-sample interaction (the *dashed orange line*) at small tip-sample distances, leading to an overall reduction of oscillation frequency (as represented by the *red line*). The gray ball is used to represent the oscillatory motion of the tip based on symmetric (*dotted blue line*) and modified (*straight red line*) potentials (Figure reproduced from Ref. [22])

Despite the success of contact-mode AFM in imaging the nanoscale structure of a number of material surfaces [19], the technique naturally requires the formation of a permanent, albeit *light* contact between the probe tip apex and the sample surface comprising of tens to hundreds of atoms (Fig. 8.1a). Since an initially atomically sharp probe tip apex becomes considerably more blunt due to the formation of the contact, averaging of the force interactions occurring between the atoms of the probe apex and the sample surface over the contact area consequently prevents *true* atomic resolution imaging, leading to an inability to detect single atomic defects such as individual vacancies on the material surface. Instead, apparent atomic-scale images obtained in contact-mode AFM shortly after its introduction have been later understood to demonstrate only the lattice periodicity of the surface under investigation [20, 21].

In order to achieve true atomic resolution imaging using an AFM-based approach, a new *dynamic* operation mode has been introduced in 1995 [23–26]. As opposed to the *static* operation associated with contact-mode AFM, the micromachined cantilever to which the tip apex is attached is oscillated at its resonance frequency in the new, *noncontact AFM* mode (NC-AFM) [27–33]. In typical NC-AFM operation, the tip is brought into close proximity of the surface in the attractive interaction regime while the cantilever is oscillating and changes in the resonance frequency induced by atomic-scale force interactions between the probe apex and the sample surface are detected as the oscillation amplitude is kept constant using a feedback loop in the so-called *frequency-modulation* (FM) operation [34]. As actual contact with the surface is prevented, the tip apex remains atomically sharp (Fig. 8.1b) and site-specific variations in frequency shift detected during precise raster-scanning over the sample surface result in the acquisition of true atomic-resolution maps reflecting the structure of the surface. Since its first successful application for atomic-resolution imaging in 1995 [23–26], the method of NC-AFM has delivered atomically resolved maps of a large number of surfaces, including semiconductors [35–46], metals [47–50], and insulators [51–60]. Moreover, in recent years, well-defined functionalization of the probe tip apex with adsorbed molecules such as CO and partial operation in the repulsive interaction regime have resulted in the acquisition of very high-resolution spatial maps on adsorbed organic molecules on surfaces so that individual atoms and bonds inside the molecules have been clearly observed [61–64].

Since NC-AFM directly utilizes the effect of chemical interactions acting between the probe tip and the sample surface on the oscillation characteristics of a micromachined cantilever to perform atomic-resolution imaging, it is natural to expect that the method can also be used towards the quantification of those interactions in terms of forces and energies. Unfortunately, despite the fact that the connection between frequency shifts (the main parameter relevant for NC-AFM imaging) and interaction forces and energies can be expressed mathematically, the associated calculations require acquisition of the frequency shift values from the point of interest above the surface all the way to a distance where the cantilever oscillation is unaffected by interactions with the surface [65–70]. As such, the determination of interaction forces and energies quantitatively above a given atomic site on the material surface starts with the recording of a frequency shift-distance curve in the vertical direction. Consequent conversion of the acquired frequency shift data mathematically into a force/energy curve using the above-mentioned methods thus forms the essence of force spectroscopy, which has been demonstrated in a number of studies in the past [71–77]. As a natural extension of the described technique, combination of a large number of spectroscopy curves acquired at different locations on a given sample surface into 2D and 3D maps of interaction forces and energies has been realized as well [78–87], thanks to advancements in instrumentation and acquisition methods [88].

In the following sections of the present chapter, an overview regarding experimental and instrumental methodology associated with the NC-AFM technique will

be provided, followed by a review of key research findings associated with atomic-resolution imaging of various material surfaces, as well as atomic-resolution force spectroscopy. The chapter will conclude with an outlook regarding potential directions for future NC-AFM research. While the NC-AFM community was initially small, it is growing with each passing year and as such, the number of reported results rapidly increases, as well. While an effort has been made to include a majority of published results regarding various aspects of NC-AFM research in this chapter, we apologize for any unintended omissions.

4 Experimental and Instrumental Methodology

Shortly after the introduction of the STM, it was apparent that interaction forces acting between the metallic probe tip apex and the sample surfaces under investigation led to certain distortions in acquired data [89]. As such, the possibility of detecting interaction forces between atoms at such small length scales has been investigated, resulting in the invention of the AFM [5]. As described in the previous section, it became ultimately apparent that AFM in its traditional manifestation of contact-mode was unable to achieve true atomic-resolution due to the finite contact area that forms between the probe apex and the sample surface, leading to the introduction of *dynamic* operation modes, where the cantilever is oscillated at or near its resonance frequency as opposed to static operation in the contact mode [29]. Dynamically operating an atomic force microscope can be accomplished in two different ways: amplitude modulation (AM) or frequency modulation (FM). AM-AFM – where the cantilever is oscillated with a fixed driving frequency near resonance and changes in its amplitude and phase characteristics based on changing tip-sample distance are used as the detection signal [90, 91] – has been mainly used in the literature towards the goal of nanometer-scale imaging in liquid and ambient conditions due to the relatively long timescales associated with the response of high quality factor (Q) cantilevers which are needed for atomic resolution imaging with low imaging noise [29, 92]. As opposed to AM-AFM, during FM-AFM operation the cantilever is oscillated at resonance (f_0) and the magnitude of the oscillation amplitude (A) is kept constant by the utilization of a feedback loop [34]. As the cantilever base is approached to the sample surface under investigation, the resonance frequency of the cantilever shifts to a new value f due to the interactions of the tip apex atoms with the atoms of the surface, and the associated shift in resonance frequency (referred to as *frequency shift*, $\Delta f = f - f_0$) is used as the main imaging signal. A second feedback loop is utilized to keep the frequency shift at a fixed value by changing the vertical position of the cantilever base accordingly while the surface is being raster-scanned by the probe tip with picometer resolution and so atomic-resolution topographical maps of any flat sample surface irrespective of electrical conductivity (as opposed to STM) can be obtained. As atomic-resolution NC-AFM studies have been almost exclusively performed in the FM mode in the literature (with the exception of a few cases [93]), the use of the term "NC-AFM" in the AFM community is usually taken to imply FM operation.

Interactions of the probe tip with the sample surface leading to the frequency shift can be classified as long-range and short-range. While electrostatic interactions occurring due to potential differences between the probe tip and the samples surface as well as the ubiquitous van der Waals interaction due to spontaneous fluctuations leading to dipoles act at long range and cause generally a diffuse background signal in NC-AFM images, the site-specific chemical interactions relevant for atomic-resolution imaging (usually described by empirical models such as those by Morse and Lennard-Jones) [94] are generally of short-range character [73, 77, 84]. It needs to pointed out that while atomic-resolution imaging with NC-AFM has been traditionally performed mainly in the attractive interaction regime [27], recently it has been demonstrated that partial operation in the repulsive regime with small amplitudes results in the acquisition of very high-resolution images on adsorbed organic molecules, revealing the intramolecular structure with unprecedented precision based on minute differences in site-specific Pauli repulsion forces [61, 95].

Mechanical properties of cantilevers employed in NC-AFM (spring constant k, resonance frequency f_0 and quality factor Q) affect oscillation characteristics and consequently, the acquired data. While in the initial manifestation of NC-AFM, cantilevers with relatively low stiffness values (few tens of N/m or less) have been employed with large oscillation amplitudes ($\sim$10 nm) to perform atomic resolution imaging [23, 47, 96, 97], the use of tuning forks with much higher stiffness ($\sim$2,000 N/m) in conjunction with lower oscillation amplitudes ($\sim$1 nm) in the so-called *q-Plus* mode has emerged as an exciting alternative [80, 84, 86, 98–101]. The main advantages associated with the use of tuning forks in NC-AFM experiments can be summarized as the ability to operate at low amplitudes without instabilities related to the *jump-to-contact* phenomenon due to increased stiffness, increased sensitivity to short range interaction forces due to reduced amplitudes [102], the ability to freely choose the tip material by utilizing cleaved or electrochemically etched thin metallic wires attached to one of the prongs, as well as the electrical detection of the oscillating signal based on the piezoelectric character of quartz, eliminating the need for optical detection equipment in the microscope [30].

As indicated in the previous section, one of the main strengths of NC-AFM is based on the fact that it can be utilized towards performing site-specific interaction force and energy spectroscopy on the material surface of interest [71–88]. The acquisition of individual curves of frequency shift versus tip-sample distance and the consequent conversion into force and energy follows established procedures. At this point, it should be indicated that various mathematical approaches have been put forward in the literature to describe the relation between frequency shifts measured in NC-AFM spectroscopy experiments as a function of tip-sample distance and the interaction forces that cause them [65–70]. While some of the methods used to calculate interaction forces from measured frequency shift data are valid only for relatively large amplitudes (>5 nm), the method of Sader and Jarvis is usually preferred due to the fact that it provides a good approximation for all amplitude regimes and that its solution is relatively easy to implement

computationally [68]. According to this approach, the interaction force F acting between the tip and sample in the vertical direction at a distance of z is given by

$$F(z) = 2k\int_{z}^{\infty}\left(1+\frac{\sqrt{A}}{8\sqrt{\pi(u-z)}}\right)\frac{\Delta f(u)}{f_0} - \frac{A^{3/2}}{\sqrt{2(u-z)}}\frac{d}{du}\left(\frac{\Delta f(u)}{f_0}\right)du$$

Once again, it should be pointed out that the calculation of the interaction force at a given tip-sample distance requires knowledge of all frequency shifts form the distance of interest all the way to a separation where tip-sample interactions are negligibly small, as seen from the mathematical expression above. After conversion to force F has been performed for a single spectroscopy curve, interaction energy values are simply obtained by numerically integrating the force data. Since short-range chemical forces are mainly thought to be responsible for atomic-resolution imaging and spectroscopy in NC-AFM experiments on reactive surfaces [103, 104], appropriate methods have been proposed to eliminate the contribution of long-range interactions from the experimentally measured total force [105, 106]. Accordingly, compensating for the contact potential difference between the tip and sample by the application of a bias voltage and subsequent subtraction from the total force interaction eliminates the long-range electrostatic force contribution. Moreover, the fitting of a Hamaker-type interaction model to the long-range part of measured force spectroscopy curves assuming a sphere-plane geometry (where the radius of the sphere represents the radius of curvature associated with the apex of the tip employed in the experiments) and subsequent subtraction from the total force interaction eliminates the effect of van der Waals interactions.

Based on the methods established in the literature regarding spectroscopic data acquisition and subsequent conversion into forces and energies, various approaches have been suggested and utilized for the acquisition of two/three-dimensional interaction force and energy data [88]: While the *curve-by-curve* acquisition method depends on recording multiple spectroscopy curves one by one and their subsequent combination into a single two/three-dimensional map, i.e., Refs. [78, 79, 87, 107–110] the *layer-by-layer* method involves the recording of several NC-AFM images with slow topography feedback at various semi-constant heights above the sample surface (Fig. 8.2) i.e., Refs. [84, 86, 87, 111, 112]. The individual layers of data can be then manually drift-corrected and combined into a single three-dimensional map of interaction forces or energies. While both techniques feature certain advantages and disadvantages, it should be stated that the *curve-by-curve* method necessitates the use atom-tracking/feedforward methods [113, 114] in order to collect drift-corrected data, while the layer-by-layer method allows post-acquisition drift correction, which is additionally facilitated at low temperatures [88].

As expected, atomic resolution imaging and force spectroscopy experiments performed using NC-AFM are readily affected by the structural and chemical

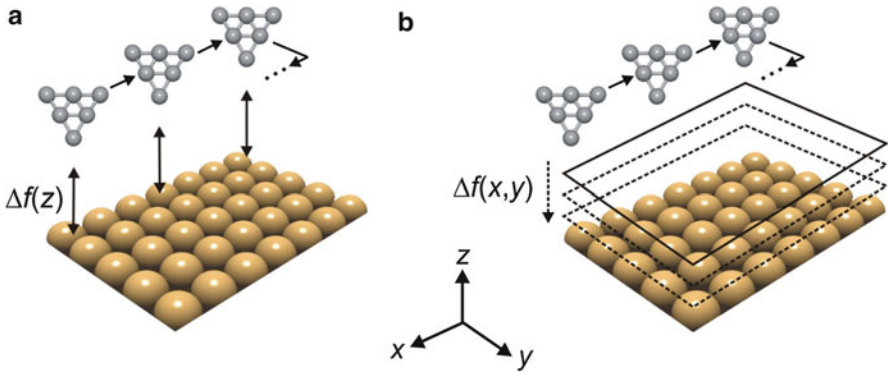

Fig. 8.2 Schematic illustrations describing acquisition procedures used to collect site-specific frequency shift data on material surfaces: While the *curve-by-curve* approach is based on the recording of individual $\Delta f(z)$ curves (**a**), separate NC-AFM images at semi-constant heights above the surface are collected in the *layer-by-layer* approach (**b**) (Figure reproduced from Ref. [88])

properties of the tip apices employed in the experiments [31, 61, 115–121]. While the effect of tip asymmetry and elasticity on NC-AFM experiments have been the subject of a few numerical studies in recent years [88, 122], more effort needs to be spent in this direction if a standardization of atomic-resolution imaging and especially spectroscopy experiments is to be achieved. An interesting experimental approach towards standardization of the chemical and structural properties have been realized through the adsorption of a well-defined single molecule such as CO on the tip apex, delivering several very promising results in terms of increased spatial resolution [61, 62, 123].

It should also be noted that atomic resolution imaging and spectroscopy experiments on material surfaces of interest using NC-AFM are significantly facilitated by the utilization of low temperatures (achieved by the use of liquid nitrogen or helium) and operation under ultrahigh vacuum (UHV) conditions [73, 124]. While operation at low temperatures delivers higher levels of stability with decreased thermal drift and piezo nonlinearity effects as well as improved quality factors leading to high signal-to-noise ratios, ultrahigh vacuum conditions ensure the atomic-scale cleanliness of the sample surface for long durations by dramatically reducing the number of adsorbed molecules on the sample surface [27]. Despite the advantages provided by low temperature operation under UHV for NC-AFM experiments, the development of methods such as atom tracking [113] in combination with the feedforward methodology [114] now allow virtually drift-free imaging and spectroscopy experiments at room temperature [87, 107, 108, 125]. Additionally, it should be stated that in recent years, the relatively small niche area of atomic-resolution experiments in UHV conditions has been expanded by successful demonstration of atomic-resolution imaging and spectroscopy under liquids as well as ambient conditions via major advances in instrumentation and methodology [126–133].

5 Key Research Findings

5.1 Atomic-Resolution Imaging

5.1.1 Semiconductor Surfaces

Due to their wide-spread use in the electronics industry, silicon and related semiconductor materials are of great scientific, technological and industrial importance. Therefore, it is only natural that the prototypical Si(111)-7×7 surface has been the focus of initial NC-AFM studies where atomic-resolution was demonstrated in 1995 under UHV conditions by the utilization of a frequency modulation approach [23, 25]. During the same year, research efforts by the group of S. Morita in Osaka University culminated in the atomic-resolution imaging of the InP(110) surface and the observation of point defect motion at room temperature [24, 26]. Following these spectacular results constituting a "proof-of-principle" for true atomic-resolution imaging via NC-AFM, multiple research groups have succeeded in obtaining atomic-resolution images of the Si(111)-7×7 surface using different microscope setups [134–136]. Despite the fact that the Si(111)-7×7 surface was one of the first to be imaged with atomic-resolution via NC-AFM and is nowadays frequently employed as a "test sample" to investigate the capabilities of custom-built and commercial instruments, several interesting results continue to be reported on this sample system, such as the observation of subsurface atoms [137] as well as differences in contrast formation mechanisms observed during combined NC-AFM/STM studies [138].

Another sample system based on the semiconducting Si(111) surface that has been characterized to a certain extent by NC-AFM experiments is the $Ag:Si(111)-\left(\sqrt{3}\times\sqrt{3}\right)R30^{o}$ surface obtained by deposition of Ag atoms on a Si(111) surface under UHV conditions and at elevated temperatures [40, 43, 46]. The atomic-scale investigations on this sample are motivated by a general interest in metal–semiconductor interfaces as well as the fact that the precise atomic structure of the surface has remained a matter of debate in the scientific community. Earlier investigations at room temperature have revealed that the atomic-scale contrast observed in NC-AFM experiments changes based on varying tip-sample distance and it was concluded that a so-called *honeycomb-chained-trimer* (HCT) model describes the surface structure satisfactorily [40, 46]. However, an extensive study of combined NC-AFM and STM experiments performed at variable temperatures have later revealed that the ground state surface structure is explained by an *inequivalent trimer* (IET) model at low temperatures and the appearance of a HCT-type structure at room temperature is due to a thermal averaging (fluctuation) effect [43]. Thus, the exciting potential of the NC-AFM method in atomic-scale structural characterization of semiconducting surfaces is clearly demonstrated.

Due to its importance for the electronics industry and micro-fabrication technologies, the Si(100) surface has also been targeted by NC-AFM measurements aimed at uncovering its atomic-scale structure in real space [35, 41, 44, 139–143].

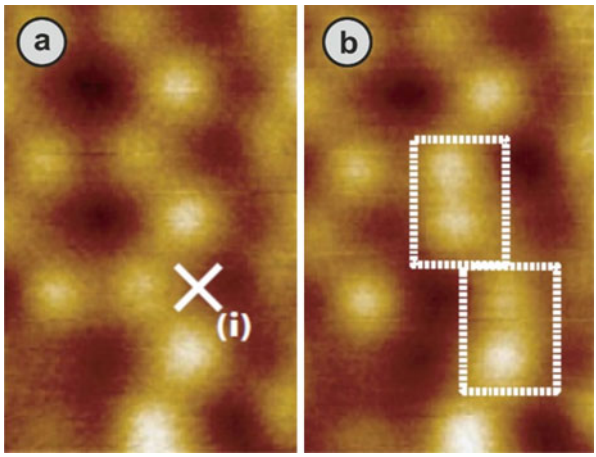

Fig. 8.3 NC-AFM images of the semiconducting Si(100) surface acquired at a temperature of 5 K. While atomic arrangement of the surface in the $c(4\times2)$ reconstruction is imaged in (**a**), controlled approach of the tip to the location indicated by (*i*) leads to *dimer flipping*, as indicated by the rectangles in (**b**) (Figure reproduced from Ref. [141]. Copyright (2011) by the American Physical Society)

While measurements performed at low temperatures have confirmed that the ground state of the surface is characterized by buckled Si dimers with tilted bonds leading to a $c(4\times2)$ reconstruction [139], thermal fluctuations between stable buckling positions for each dimer lead to an apparent $p(2\times1)$ surface structure at room temperature [35]. Even more interestingly, Li et al. have determined that tip-induced interaction forces at small tip-sample distances during NC-AFM imaging induce dimer flipping, leading to the occasional observation of a $p(2\times1)$ reconstruction during low temperature experiments [44]. Further, careful experiments by Sweetman et al. have culminated in the deliberate flipping of single dimers on the Si(100) surface at zero bias voltage and low temperatures by controlling the magnitude of the tip-sample interaction, essentially demonstrating pure mechanical toggling of an atomic scale switch (Fig. 8.3) [140, 141].

In order to evaluate the ability of NC-AFM to discriminate the chemical identity of multiple atomic species on a given surface, semiconductor alloy surfaces consisting of combinations of Si, Sn, In, Ge and Pb atoms have been investigated via imaging experiments [144–147]. The results remarkably show that the NC-AFM method is clearly able to distinguish one type of atom from the other by detecting differences in measured topographic height (Fig. 8.4). Evaluating the recorded images in conjunction with careful force spectroscopy measurements then allows the assignment of the detected height difference to atomic scale relaxations as well as differences in short-range interaction forces exhibited by each type of atom with the probe tip. Finally, by utilizing a combination of experimental results and ab initio calculations, a procedure for chemical identification of individual atoms regardless of the specifics of experimental parameters and tip apex properties has been introduced (for details, see Sect. 5.2.1; [77]).

Results related to atomic-resolution imaging of semiconductor surfaces are not limited to the examples discussed above. Indeed, excellent atomic-scale structural data has been presented on Ge(111) [39, 148] and Ge(001) [45], GaAs(110) [38], and InAs (110) [149]. Based on the discussion in this section, it is clearly seen that NC-AFM has

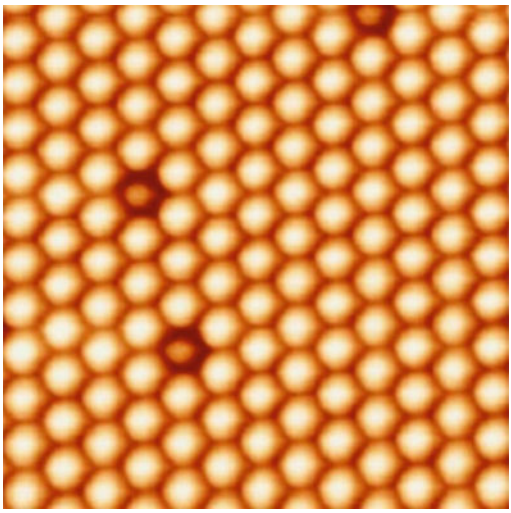

Fig. 8.4 Topographic NC-AFM image of a Sn/Si (111) alloy surface (8.5 nm^2 × 8.5 nm^2) where differences in the chemical identity of individual atoms lead to clear changes in image contrast (Figure reproduced from Ref. [147]. Copyright (2006) by the American Physical Society)

been established as a prominent tool for atomic-scale characterization of semiconductor surfaces. In the following sections, application of the NC-AFM method to other surfaces of scientific interest (metal oxides, ionic crystals, etc.) will be covered.

5.1.2 Metal Oxide Surfaces

Shortly after the first demonstration of the atomic-resolution capability of NC-AFM on the surface of Si(111)-7×7, efforts have been directed at resolving the atomic structure of surfaces associated with other materials. Of the different classes of materials that have been investigated with NC-AFM, metal oxides are of particular interest due to (a) their wide application in diverse fields such as electronics, heterogeneous catalysis and biomedical engineering and (b) the fact that most metal oxides of technological interest are electrical insulators and as such, the associated surfaces cannot be probed with ease using standard surface science techniques relying on the utilization of freely moving electrons [150]. Therefore, prior to the introduction of NC-AFM as a surface characterization tool with atomic-resolution imaging capability, experimental studies aimed at atomic-resolution imaging of metal oxide surfaces using STM have been closely restricted to partially reduced, semiconducting metal oxide samples (e.g., rutile TiO_2(110) [151]) and thin films on conducting substrates [152].

Based on growing scientific and technological interest in the surface structure and properties of metal oxides, NC-AFM has been utilized towards atomic-resolution imaging of surfaces associated with a number of insulating and semiconducting metal oxides (including thin oxide films) such as TiO_2 [96, 115, 118, 120, 121, 153–156], Al_2O_3 [52, 157–163], CeO_2 [57, 164–169], NiO [170–174], MgO [162, 175–177], ZnO [178], MoO_3 [179], and $MgAl_2O_4$ [59, 180, 181], as well as thin layers formed through oxidation of metal substrates [86, 182] in the past two decades. While an excellent and exhaustive review of the subject has been published previously [183], in

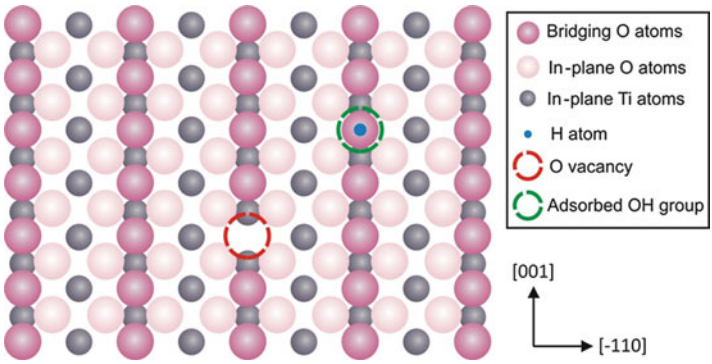

Fig. 8.5 Structural model of the rutile $TiO_2(110)$ surface with *regular* defects. In-plane oxygens are threefold coordinated, whereas bridging oxygens are twofold coordinated. Ti sites under the bridging oxygens are sixfold, and the exposed ones are fivefold coordinated

this chapter we will present the development of atomic-resolution imaging on metal oxide surfaces via NC-AFM with the example of rutile $TiO_2(110)$, which is by far the most widely studied metal oxide surface via a host of surface science techniques, in addition to being of high importance for photocatalysis applications [151, 184].

Even though the anatase form of TiO_2 is more relevant for practical catalysis applications, rutile $TiO_2(110)$ has been the focus of most NC-AFM imaging experiments due to the fact that its structure and the types of common defects encountered are very well known and have been well documented in the literature [151]. As shown in Fig. 8.5, the rutile $TiO_2(110)$ surface is composed of alternating rows of five and sixfold coordinated Ti^{4+} cations and threefold coordinated *in-plane* O^{2-} anions, as well as rows of *bridging* O^{2-} anions that are twofold coordinated. Whereas the bulk unit cell has a tetragonal structure with $a = b = 0.4584$ nm and $c = 0.2953$ nm [151], the distance between two rows of *bridging* O^{2-} anions or fivefold coordinated Ti^{4+} cations on the (110) face is 0.65 nm, while a monoatomic step is 0.325 nm high [185]. The types of defects which are commonly encountered on the rutile (110) surface after conventional UHV preparation (involving sputter/anneal cycles) include O vacancies on *bridging* O^{2-} rows, as well as OH groups forming on such vacancies due to H_2O dissociation a few hours after sample preparation, even under very good UHV conditions [121, 186].

While the contrast observed in typical STM images of $TiO_2(110)$ [185–188] has been well understood (bright stripes coinciding with rows of fivefold Ti^{4+} ions, and bright protrusions in between corresponding either to O vacancies or OH groups) [151]. NC-AFM images have shown a much larger variety of contrasts ever since the first atomic-resolution measurements have been performed on $TiO_2(110)$ using this technique [96]. The overall consensus in the literature so far is that there are three most common contrast types observed in NC-AFM measurements of $TiO_2(110)$ [120, 121]: (1) The *protrusion* mode, where Ti rows are imaged as bright stripes and O vacancies and OH groups are imaged as bright protrusions between the stripes. (2) The *hole* mode, where bridging O^{2-} rows are imaged as

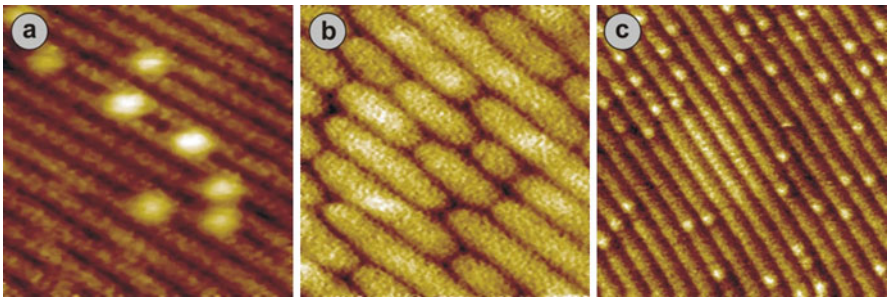

Fig. 8.6 The three common imaging modes that are frequently encountered in NC-AFM measurements: the *protrusion* (**a**), *hole* (**b**), and *neutral* (**c**) modes. In the protrusion mode, bright stripes coincide with fivefold Ti^{4+} sites on the surface and regular defects are imaged as protrusions between the stripes. For both hole and neutral modes, bright stripes coincide with bridging oxygen sites. Whereas the hole mode displays regular defects as depressions on bright stripes, the neutral mode resembles the *real* topography of the oxide surface (Figure reproduced from Ref. [121]. Copyright (2007) by the American Physical Society)

bright and O vacancies/OH groups as dark depressions on these rows. (3) The *neutral* mode where AFM images tend to reflect the real topography of the sample surface: In this imaging mode, bridging O^{2-} rows are imaged as bright stripes, OH groups as bright protrusions on top of these rows and O vacancies as dark depressions on the same rows. The extensive NC-AFM work performed in F. Besenbacher's group at Aarhus University in collaboration with DFT simulations has led to the conclusion that these contrast types can be generally explained by the different electronic *polarities* of the tip apices used in the experiments: [120, 121] (1) A negatively charged anion at the tip apex (e.g., O^{2-}) would interact more strongly with the positively charged Ti^{4+} ions on the surface due to local electrostatic interaction and produce images where rows of Ti^{4+} ions are imaged as bright stripes. Moreover, since O vacancies and OH groups might be thought of as electrostatically *less negative* than regular O^{2-} anions, they are imaged as bright protrusions on dark O^{2-} rows (*protrusion* mode). (2) Similarly, a positively charged cation at the tip apex (e.g. Ti^{4+}) would interact more strongly with the negatively charged O^{2-} ions on the surface due to electrostatic interaction and produce images where rows of O^{2-} ions are imaged as bright stripes, with O vacancies/OH groups as depressions on these rows due to weaker electrostatic attraction to the tip apex (the *hole* mode). (3) Lastly, a *neutral* tip apex (such as a pure Si tip that has not been pre-treated by light crashes with the TiO_2(110) surface, thus terminated by Si atoms), would interact mostly via covalent bonds with the surface atoms and produce images representing the true topography of the sample surface, as corroborated by DFT simulations (the *neutral* mode) [121, 189]. A comparison of all contrast modes discussed here for NC-AFM imaging is given in Fig. 8.6.

It should be noted here that a few additional NC-AFM studies performed by other research groups have revealed the existence of additional, more *exotic* imaging modes. Specifically, Yurtsever et al. have been able to observe bright rows of O^{2-} ions with no apparent OH groups that usually cover TiO_2(110) surfaces a few hours

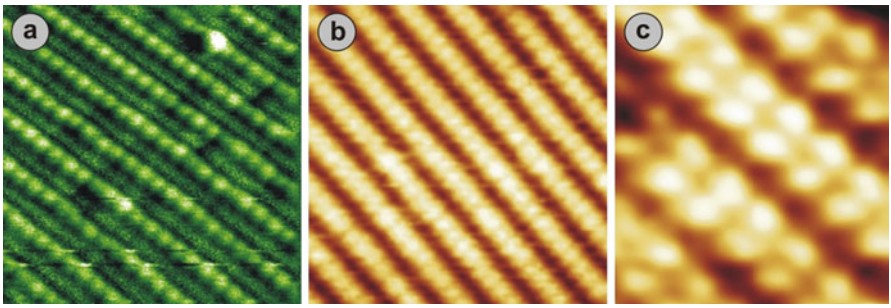

Fig. 8.7 A summary of the more *exotic* imaging modes associated with NC-AFM experiments on TiO_2(110). (**a**) The so-called *all-inclusive* mode where both bridging oxygens as well as fivefold Ti^{4+} sites are imaged as bright protrusions. (**b**) The *hidden* mode where adsorbed OH groups are not detected in NC-AFM images showing bright protrusions associated with bridging oxygen sites. (**c**) A rather rare NC-AFM image exhibiting in-plane oxygens as bright protrusions. ((**a**) reproduced from reference [118]. (**b**) and (**c**) reproduced from Ref. [155]. © IOP Publishing. Reproduced with permission. All rights reserved.)

after cleaning in UHV (the so-called *hidden* mode) [155]. Additional imaging modes observed in NC-AFM include the imaging of *in-plane* oxygens as bright protrusions [155], as well as an *all-inclusive* mode observed by Bechstein et al. [118], where both bridging O^{2-} as well as fivefold Ti^{4+} ions are imaged simultaneously as bright protrusions in NC-AFM. The all-inclusive imaging mode might be explained by the existence of a Si(100) tip with a dimer-like apex including an adsorbed O atom or OH group [116]. Regardless of the specific details associated with each of the experiments discussed in this paragraph, the results presented (and summarized in Fig. 8.7) lead to the conclusion that a simple electrostatic view of tip apices (positive, negative, or neutral) might not always be sufficient to explain all contrast types observed in NC-AFM imaging of metal oxide surfaces such as TiO_2(110). In fact, a combination of force spectroscopy experiments and ab initio simulations have been recently utilized to identify the tip apex structures responsible for commonly observed contrast modes on TiO_2(110), with the conclusion that flexible tip apices contaminated with clusters from the surface quantitatively explain the experimental imaging and spectroscopy results [156].

Finally, combined NC-AFM/STM studies have been performed on the TiO_2(110) surface to elucidate the role of the tip in contrast formation for both imaging channels [115]. Specifically, all three general modes of NC-AFM imaging (the protrusion, hole, and neutral modes) are observed in the AFM channel, with simultaneous STM images showing either *in-phase* (bright rows in AFM correspond with bright rows in STM) or *out-of-phase* character (bright rows in AFM correspond with dark rows in STM). Figure 8.8 can be consulted in order to compare the various contrasts that are obtainable in simultaneous AFM/STM imaging of TiO_2(110). Having such a variety of image contrasts available, identification of tip apices associated with each mode using DFT simulations requires considerable effort [190]. Additionally, simultaneous NC-AFM/STM

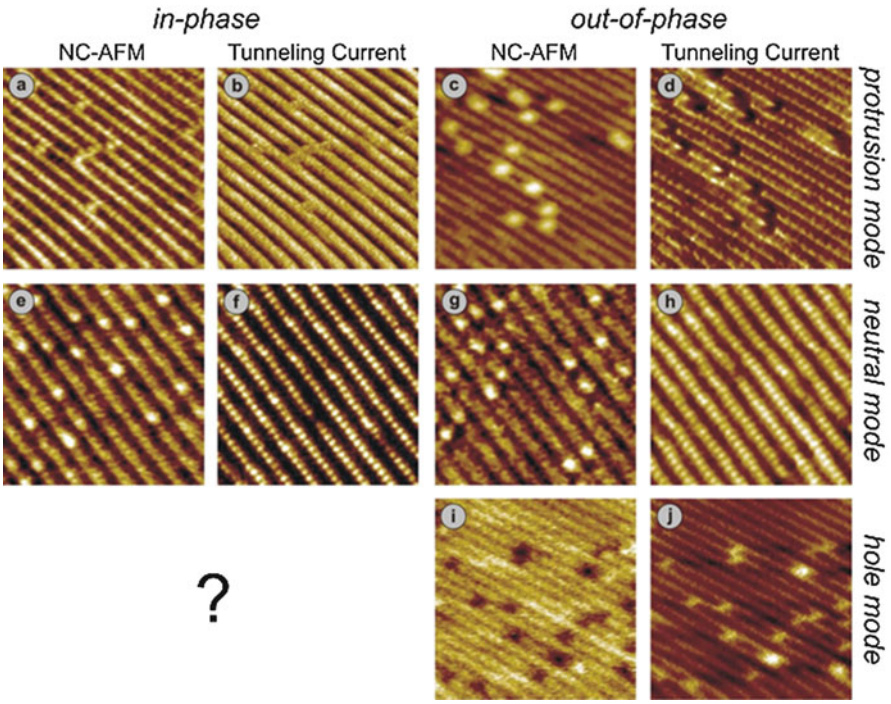

Fig. 8.8 Various imaging modes attainable in simultaneous NC-AFM/STM measurements on the TiO_2(110) surface. All combinations of the typical NC-AFM imaging modes (protrusion (**a**–**d**), hole (**i**–**j**), and neutral (**e**–**h**)) with in-phase and out-of-phase tunneling current imaging are attained in this study, except for the in-phase recording of tunneling current data for hole mode NC-AFM imaging (Figure reproduced from Ref. [115]. Copyright (2008) by the American Physical Society)

measurements have revealed the existence of a subsurface defect in the form of an interstitial H atom, which has a characteristic electronic signature in the STM channel, but is practically undetectable with AFM [154].

Overall, the key role that NC-AFM plays in atomic-resolution characterization of metal oxide surfaces is clearly demonstrated by the representative example of the rutile TiO_2(110) surface presented in this section, together with the significant effect of tip structure and chemistry on the experiments. Taking into account that metal oxide surfaces continue to be an integral component of technical development in a number of fields, it is natural to expect that in the near future, the application of NC-AFM imaging will spread to new metal oxides beyond the classic examples of TiO_2, Al_2O_3, CeO_2, NiO, etc. mentioned previously.

5.1.3 Ionic Crystal Surfaces

Another class of materials that have been studied in detail via NC-AFM imaging experiments are ionic crystals such as NaCl, KBr, and CaF_2 [53, 54, 60, 74, 111, 191–201]. The main interest in studying the atomic structure of ionic crystal surfaces is based on three factors: (i) Ease of sample preparation through simple

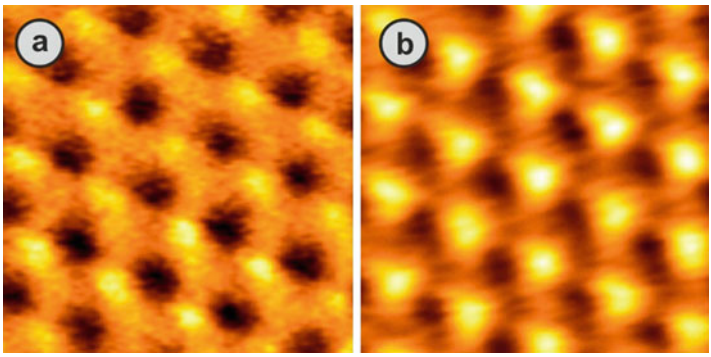

Fig. 8.9 Constant height NC-AFM images of the ionic $CaF_2(111)$ surface acquired with a tuning fork sensor in the *qPlus* configuration (1.36 nm × 1.36 nm). The image contrast reflects the frequency shift. While (**a**) has been acquired in the attractive interaction regime, (**b**) has been recorded in the repulsive regime, resulting in a reversal of contrast (Figure reproduced from Ref. [198]. © IOP Publishing. Reproduced with permission. All rights reserved.)

cleaving, (ii) the fact that the physical properties associated with their bulk structure have been studied for a very long time and (iii) the fact that they constitute model insulating substrate systems for the growth of metallic thin films as well as organic layers for molecular electronics.

Motivated by the mentioned factors, the first atomic resolution image of an ionic crystal surface (NaCl(001)) demonstrating the detection of point defects obtained via NC-AFM was published in 1997 [191]. NC-AFM work performed on fluoride surfaces such as $CaF_2(111)$ have later revealed the mobility of defects at room temperature and the alleviation of associated kinetics based on interaction with oxygen molecules leading to the formation of chemisorbed species, [53] as well as atomic-resolution imaging of step edges where individual ions and vacancies have been resolved [194]. Moreover, it was determined that the contrast exhibited by the imaged ions on $CaF_2(111)$ during NC-AFM experiments strongly depends on the polarity of the tip apex employed (which may spontaneously change during experiments by means of material transfer in the form of small clusters to or from the surface) by utilizing a combination of experimental results and theoretical calculations [54, 192]. The fundamental idea that contrast formation on ionic surfaces during NC-AFM experiments is dominated by atomic-scale variations in electrostatic interactions exhibited by the surface ions with the probe tip have been later supported by experimental studies aimed at imaging the $CaF_2(111)$ surface with well-characterized tip apices [119]. Finally, lateral manipulation of point defects on this sample surface were achieved via NC-AFM [197, 199] and individual surface ions were imaged using a tuning fork based detection scheme (Fig. 8.9; [198]).

Due to the fact that the cations and anions on binary ionic crystal surfaces (such as KBr and NaCl) are arranged in equivalent surface unit cells, their identification during NC-AFM imaging experiments via symmetry arguments is not possible and often considerable support from theoretical calculations is needed to achieve this goal. In order to overcome this difficulty, two main methods have been proposed where (i) the

ionic crystal is doped to a known ratio by a given impurity (such as Cl^- ions replacing a certain portion of Br^- ions in a KBr crystal) such that differences in topography between the two types of anions in NC-AFM images can be used to identify the type of ion imaged [196]. It is interesting to note that the two types of anions interact differently with the probe tip despite the fact that their formal charge states should be equivalent. Alternatively, (ii) the binary ionic crystal may be doped with divalent cations such that a new phase on the surface forms together with the introduction of point defects compensating for the charge imbalance caused by doping leading to facilitation of chemical identification of ions in NC-AFM images [202–204].

Aside from the surfaces obtained by cleaving of bulk ionic crystal samples, ultrathin films of alkali halides and fluorides grown on metal and semiconductor substrates have been targeted by atomic-resolution NC-AFM studies as well, primarily due to their potential applications in fields such as catalysis and molecular electronics [205–207]. Moreover, ultrathin films of alkali halides have been used as substrates for very high-resolution imaging of adsorbed organic molecules in studies conducted by tips functionalized with single molecules such as CO [61].

5.1.4 Other Material Surfaces and Adsorbed Molecules

In addition to semiconductors, metal oxides and ionic crystals, NC-AFM has been used to perform atomic-resolution imaging experiments on a number of other material surfaces. Examples include, but are not limited to: Surfaces of single crystal metal samples [47–50], highly oriented pyrolithic graphite (HOPG) [84, 97, 208–210], carbon nanotubes and associated metallofullerene peapods [83, 211], a film of Xe adsorbed on graphite [51], and more recently, thin films of silica (SiO_2) showing crystalline as well as vitreous structure grown on Ru(0001) substrates [212, 213], silicene grown on Ag(111) [214], and finally, graphene [215–218].

Despite the fact that the review presented in this chapter is mainly oriented towards NC-AFM based imaging and spectroscopy of bare material surfaces, the key role that the method has played in resolving the structural, physical and chemical details of single molecules and molecular layers adsorbed on various substrates should be emphasized. In addition to recent reports of unprecedented intramolecular resolution on single molecules achieved through deliberate functionalization of tip apices [61, 62, 64, 110], earlier efforts in this direction include the imaging of formate and acetate ions, terephthalic acid, perylene derivatives, C_{60}, Co-Salen, truxene, porphyrin derivatives, water, etc. adsorbed on various substrates [219–232]. As such, the potential of NC-AFM as a powerful characterization tool capable of resolving atomic-scale structural properties extends from various classes of bare material surfaces to individual molecules.

5.2 Atomic-Resolution Force Spectroscopy

5.2.1 Pioneering Studies in Atomic-Resolution Force Spectroscopy

Surfaces play a key role for a large number of scientifically and technologically relevant phenomena including friction, adhesion, corrosion, thin film growth and

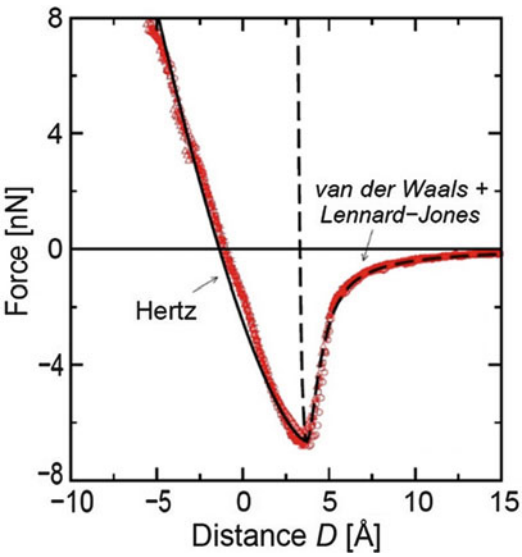

Fig. 8.10 A force spectroscopy curve obtained experimentally via the recording of frequency shift as a function of tip-sample distance using a Si tip on the HOPG surface at a temperature of 80 K. While the interaction up to the turning point is nicely approximated by the Hamaker-type van der Waals and the Lennard-Jones interaction models (*dashed line*), the interaction at closer separations obeys the Hertz contact law (*straight line*) (Figure reproduced from Ref. [71]. Copyright (2000) by the American Physical Society)

heterogeneous catalysis, among others. Considering that the interactions exhibited by atoms at the surfaces of various materials with other atoms, molecules or surfaces in their vicinity direct the physical laws that govern the processes mentioned above, the need for an experimental technique that would allow direct measurement of such interactions at atomic length scales arises. As mentioned earlier in this chapter, the method of NC-AFM, when utilized in conjunction with appropriate experimental equipment and protocols, allows to perform atomic-resolution force (and consequently, energy) spectroscopy in all three spatial dimensions above sample surfaces of interest. As such, we will review in this section key results that have been obtained with NC-AFM with regards to atomic-resolution force spectroscopy.

Shortly after the demonstration of atomic-resolution imaging on semiconductor surfaces using a frequency modulated NC-AFM approach [23–26], efforts have been directed by several research groups around the world to perform atomic-resolution force spectroscopy by measuring the tip-sample interaction force as a function of tip-sample distance above individual locations on sample surfaces [71–73, 233]. Specifically, an extensive analysis of force spectroscopy data obtained on HOPG at liquid nitrogen temperatures found good agreement between the experimental measurement and specific force laws (Hamaker-type van der Waals interaction law, Lennard-Jones type interaction law and Hertz-type contact law) (Fig. 8.10) [71]. Moreover, in a seminal work published in 2001, the scanning probe microscopy research group at University of Basel have succeeded in quantifying the short-range interaction forces associated with the onset a covalent bond between a Si tip and a Si(111)-7×7 surface using a low temperature atomic force microscope with high-stability, whereby minute differences in interactions between inequivalent atoms of the surface have also been detected [73].

The pioneering force spectroscopy experiments described above have been complemented by additional studies where force spectroscopy data obtained on different atomic sites on ionic crystal surfaces such as KBr(001), NaCl(001) and CaF_2(111) have been utilized in conjunction with ab initio simulation studies to (a) characterize in detail the structure and polarity of tip apices, (b) determine the identity of imaged ionic species, and (c) study the effects associated with atomic-scale relaxation and asymmetry of the tip apex utilized in the experiments [74, 200, 234, 235]. Moreover, the simultaneous recording of multiple data channels (such as frequency shift and tunneling current) during spectroscopy experiments have revealed varying distance dependence for the observed variables and allowed comparisons to be made regarding the physical mechanisms responsible for each [236]. In an interesting experiment, Sugimoto et al. have demonstrated that enhanced signal-to-noise ratio for frequency shift spectroscopy curves acquired at room temperature can be achieved by the use of higher flexural modes of cantilevers in conjunction with decreasing oscillation amplitudes [76]. Finally, in 2007, the goal of unambiguous chemical identification of individual atoms that form a material surface has been realized [77]: The authors, by utilizing a combination of a large number of force spectroscopy curves on alloy surfaces consisting of Si, Sn, In and Pb atoms and ab initio density functional theory calculations, have demonstrated that the largest force interactions always occur on Si atoms and the relative ratio of the maximum force interaction values between different types of atoms remains constant, despite the fact that absolute values of measured interactions do change considerably based on measurement parameters as well as chemical and structural properties of the tip apex (Fig. 8.11).

5.2.2 Three-Dimensional Force Spectroscopy with Atomic Resolution

As demonstrated by the experiments described above, the procedures for recording and processing frequency shift spectroscopy curves to obtain atomic-resolution force and energy data as a function of tip-sample distance on individual lattice sites has been well-established in the decade following the achievement of atomic-resolution imaging in NC-AFM. Consequently, the idea of combining thousands of such $\Delta f(z)$ curves to form three-dimensional data sets that allow recovering forces and energies as a function of position (x, y, z) above the sample surface seems straightforward. Performing this task with a sufficiently high number of $\Delta f(z)$ curves such that high-quality volumetric maps of interaction force and energy are obtained, is however a very challenging aim. Considering that acquiring a low-noise $\Delta f(z)$ curve takes typically about 5 s, collecting individual curves for each point on a data set consisting of 256 $\times$ 256 pixels laterally (a resolution common for NC-AFM images) should take about 90 h [237]. Due to the fact that most NC-AFM instruments operate at room temperature, thermal drift becomes an important issue, making it impossible to image the same area of the sample surface for such extended measurement times unless atom-tracking/feedforward techniques [113, 114] are employed (note that based on the microscope design and associated stability characteristics, even microscopes operating at low temperatures may feature levels of thermal drift that are not suitable for three-dimensional

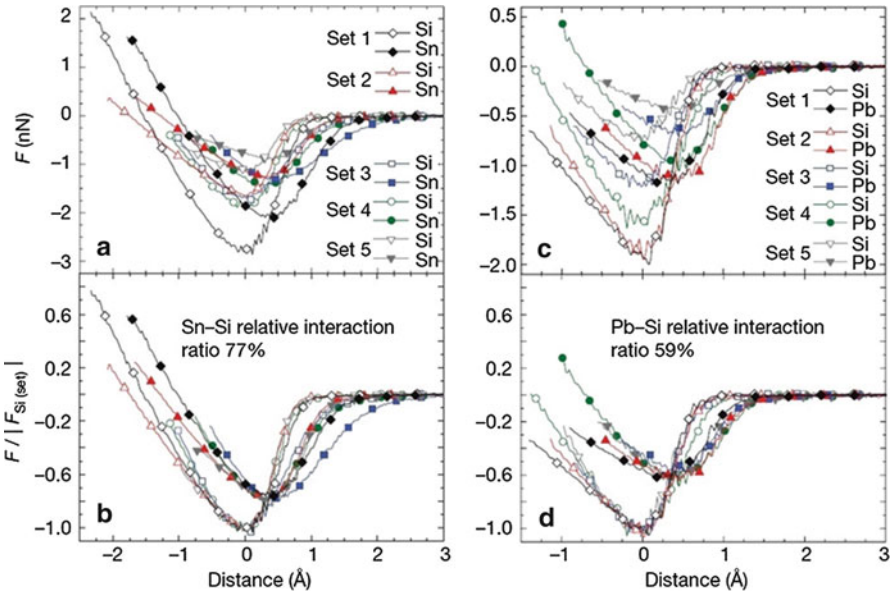

Fig. 8.11 Sets of force spectroscopy curves recorded on Si and Sn (**a**) as well as Si and Pb atoms (**c**) using NC-AFM. Despite the fact that significant differences between individual force curves can be observed due to the use of different tips, normalizing the data in each set with respect to the absolute maximum force recorded on Si $|F_{Si(set)}|$ reveals a distinct chemical signature associated with each type of atom in terms of the maximum normalized interaction force (**b**, **d**), irrespective of the specifics of the tip apex employed (Figure reproduced from Ref. [77] by permission from Macmillan Publishers Ltd, copyright (2007))

spectroscopy). Moreover, extended measurement times also increase the chance of permanent tip changes occurring at the apex, rendering the data collected up to the point of tip change unusable [237].

Due to the challenges described above, most experiments aimed at collecting full three-dimensional (volumetric) maps of interaction forces and energies above sample surfaces using NC-AFM have initially resulted in two-dimensional maps, describing the tip-sample interaction as a function of distance and lateral position in a defined crystallographic direction [78–82, 238]. While these experiments provided very useful physical information regarding, e.g., potential energy barriers [79] and lateral in addition to vertical force interactions [81], the goal of full three-dimensional atomic-resolution force spectroscopy was reached in 2009 [84]. The scanning probe microscopy group at Yale University utilized the combination of a home-built, ultrahigh vacuum and low-temperature noncontact atomic force microscope with very high stability and low drift rates (as low as 2–3 Å per day at liquid helium temperature as opposed to a typical value of a few Å per minute at room temperature) [101] and a new data acquisition and processing method to obtain a virtually drift-free map of interaction forces in three-dimensions on a 1750 pm × 810 pm area on HOPG [22, 84]. While the details of the data acquisition and

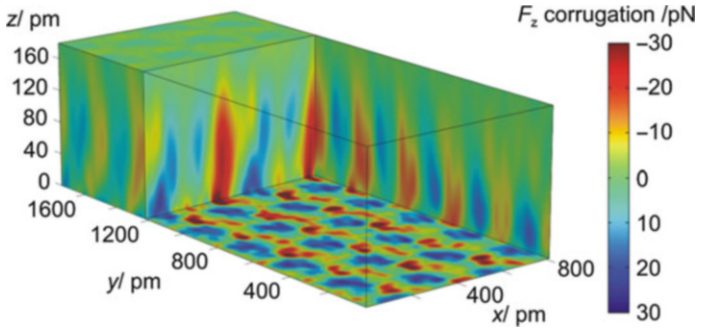

Fig. 8.12 Three-dimensional representation of the interaction force field acquired via NC-AFM based spectroscopy on HOPG. Atomic-scale corrugation on the plane of closest approach as well as the gradual weakening of interactions with increasing tip-sample distance are clearly observed. More negative values indicate more attractive interaction (Figure reproduced from Ref. [22])

processing steps as well as experimental parameters have been described elsewhere [237], the main advantage of the method lies in the fact that a *layer-by-layer* approach has been utilized instead of the typical *curve-by-curve* data collection procedure, allowing post-acquisition correction of the remaining drift to be performed manually after the experiment is finished. In the layer-by-layer approach, as described in Sect. 4 of this chapter, a series of regular, topographic NC-AFM images (together with the error signal in terms of deviations from the Δf setpoint) is collected at semi-constant heights above the sample surface with slow topography feedback, manual correction of lateral drift (which has been dramatically reduced thanks to the stable microscope design and low temperature operation) is performed image by image by cropping the part of each image that is common to all layers, and the resulting layers of topography and Δf information are combined to form a full three-dimensional set of spectroscopy data. The post-acquisition drift correction procedures also eliminates artifacts associated with the overall elastic deflection of asymmetric tip apices with increasing vertical forces as the tip-sample distance is decreased [237].

Once a full, drift-free three-dimensional map of frequency shifts is acquired as described above (in ∼40 h, at $T = 6$ K and under UHV conditions, using a tuning fork in the *qPlus* configuration with an etched Pt/Ir tip and featuring a data density of 6.8 pm laterally and ∼2 pm vertically), the data are converted to interaction force using appropriate mathematical procedures [68]. A three-dimensional visualization of the vertical interaction force field obtained in this way is presented in Fig. 8.12 (please note that the average force value for each height has been subtracted to enhance the contrast). The average interaction force observed in the bottom plane is ∼2.35 nN and the total corrugation is ∼70 pN. One can also clearly observe atomic resolution in the bottom plane as well as the gradual weakening of the interaction with increasing tip-sample distance.

For a more detailed analysis, *cuts* of forces along any direction can now be produced to study the evolution of interaction forces as a function of lateral position on the surface using horizontal cuts as well as tip-sample distance using vertical

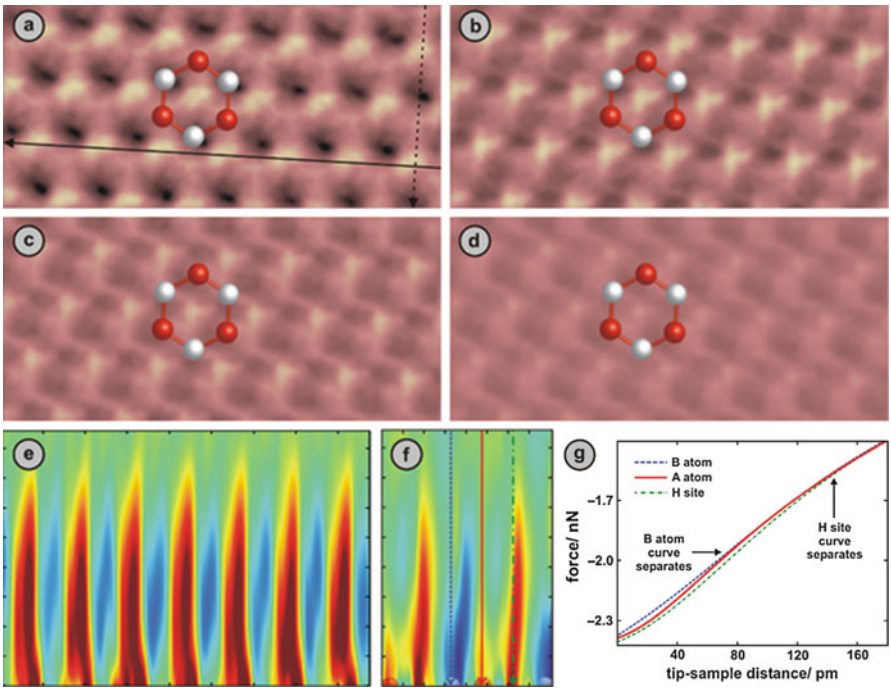

Fig. 8.13 (**a**–**d**) Horizontal force maps at 12 pm (**a**), 52 pm (**b**), 97 pm (**c**), and 132 pm (**d**) above the plane of closest approach reproduced from the three-dimensional data in Fig. 8.12. The hexagon designates the positions of the two types of inequivalent C atoms on the top layer of HOPG (A (red) and B (white) atoms). (**e**–**f**) Vertical force maps along the *straight* (**e**) and *dashed* (**f**) arrows in (**a**). (**g**) Three force spectroscopy curves recorded on the hollow lattice site (H site) as well as on top of the A and B atoms indicated in (**f**), highlighting site-specific differences in interaction forces (Figure reproduced from Ref. [22])

cuts (Fig. 8.13). Despite the fact that the horizontal maps presented in Fig. 8.13 resemble regular, *topographical* NC-AFM images, they differ significantly from these due to the fact that the image contrast now directly reflects the *magnitude of the interaction force* as a function of lattice position at a given height above the sample surface. In contrast, individual images obtained using NC-AFM only reflect a "topography" associated with a constant frequency shift, which is of limited physical significance. It is also interesting to note that the locations of largest attractive interaction with the probe tip are situated above the *hollow* sites (H sites) of the graphite lattice (i.e., the centers of the hexagons formed by the carbon atoms) [84, 239] essentially due to the fact that the relatively small atomic spacing between carbon atoms on the top layer of graphite leads to an increased interaction with the probe tip apex om hollow locations where the apex is closely surrounded by six carbon atoms.

As described above, an alternative way to study the three-dimensional interaction force data is to produce vertical maps along crystallographic directions of

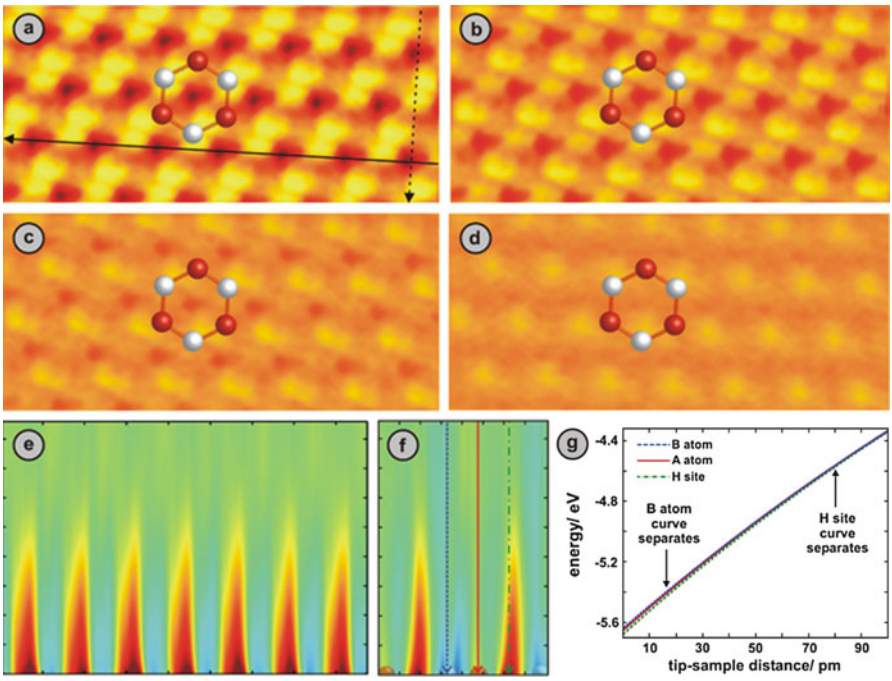

Fig. 8.14 (**a**–**d**) Horizontal maps of interaction energy corresponding to the tip-sample distances indicated in Fig. 8.13. (**e**–**f**) Vertical energy maps along the *straight* (**e**) and *dashed* (**f**) arrows in (**a**). (**g**) Three energy spectroscopy curves recorded on the hollow lattice site (H site) as well as on top of the A and B atoms indicated in (**f**). Note that the site-specific variation of interaction energy is less pronounced than force (Figure reproduced from Ref. [22])

interest. Studying the vertical force maps presented in Fig. 8.13, one can see that the atomic scale variations of the normal force on different lattice sites gradually weaken with increasing tip-sample distance and disappear at ∼150 pm above the plane of closest approach for both crystallographic directions of interest (Fig. 8.13e, f). Moreover, by extracting individual force-distance curves from the three-dimensional data on different lattice sites, the magnitude of the interactions exhibited by those sites with the probe apex can be quantified and compared as a function of tip-sample separation (see Fig. 8.13g).

As indicated before, integration of the three-dimensional interaction force data in the vertical direction results in a three-dimensional map of interaction energies, assuming that the magnitude of energy dissipation during experiments is negligible or significantly smaller than the total interaction. Analogous to Fig. 8.13, horizontal as well as vertical maps of interaction energies are presented in Fig. 8.14, together with representative curves of interaction energy versus tip-sample distance for three lattice positions of interest. It is observed that the total energy corrugation (∼0.05 eV) is less than 1 % of the maximum interaction energy observed in the bottom plane (5.7 eV). Within this context, care should be taken when comparing

quantitative results in terms of interaction forces and energies between different experiments, as the exact structure and chemistry of the tip apex have been previously found to affect NC-AFM results significantly [115–117]. The maximum interaction energy value discovered here is more than those reported for NiO (4 eV) [240] and NaCl (1.3 eV) [79], which is indicative of a rather blunt tip apex considering that graphite is a van der Waals surface and should be expected, as such, to exhibit relatively weak interactions with the probe apex. Moreover, the potential corrugation value of ~0.05 eV is smaller than the one observed for NiO (0.3 eV) [240], but similar to the one found for NaCl [79].

An important area of scientific inquiry with great technological implications is friction [241]. Despite the fact that friction is ubiquitous in our daily lives and a major source of energy dissipation in industrial processes, the basic physical laws that govern this particular phenomenon at the nanometer scale are still not well known [242]. As such, the capability of NC-AFM to perform atomic-resolution force spectroscopy to measure lateral forces acting between the probe tip and various material surfaces is of great importance. A significant advantage of NC-AFM as opposed to traditional, contact-based FFM in terms of tribological studies is that atomic-resolution information about lateral forces can be obtained thanks to the fact that the probe tip remains atomically sharp during the experiments. In contrast, since NC-AFM based force spectroscopy experiments typically probe the attractive interaction regime, direct conclusions regarding processes occurring during actual sliding events between two surfaces in contact (i.e., in the repulsive regime) cannot be made in a straightforward fashion. Still, NC-AFM has been used in the past to either directly probe frequency shifts caused by lateral forces by oscillating the tip parallel to the sample surface [243–245] or to perform two- or three-dimensional spectroscopy and then take the derivative of the resulting interaction energy field in the lateral directions x and/or y to obtain the lateral force field [81, 82, 87, 240, 246]. Moreover, in a powerful demonstration of the technique, Ternes et al. used a similar approach to calculate the magnitude of lateral forces needed for lateral manipulation of atoms and molecules on a metal surface [247]. Very recently, Weymouth et al. have utilized a tip apex terminated by a single CO atom to quantify the vertical and lateral forces experienced by the probe tip during imaging of another CO molecule adsorbed on a copper surface and have impressively managed to calculate the torsional stiffness associated with the CO molecule adsorbed on the tip apex in conjunction with a deceptively simple mechanical model [248]. Within this general context, an analysis of lateral forces in the 2009 study by Albers et al. (obtained by derivation of the interaction energy data in the lateral x and y directions) is presented in Fig. 8.15 [84, 85]. As one can clearly observe from the presented data, the structure of lateral forces detected on a horizontal plane at a fixed height above the sample surface is very different than the vertical force data: Lateral forces experienced by the atomically sharp probe tip are heavily localized around the hollow sites of the graphite lattice (where the maximum vertical forces are detected) in asymmetric rings, while the lateral force values outside of the localized rings are comparably very small. This interesting observation is further supported by zoomed images of a lateral force ring (Fig. 8.15e, f)

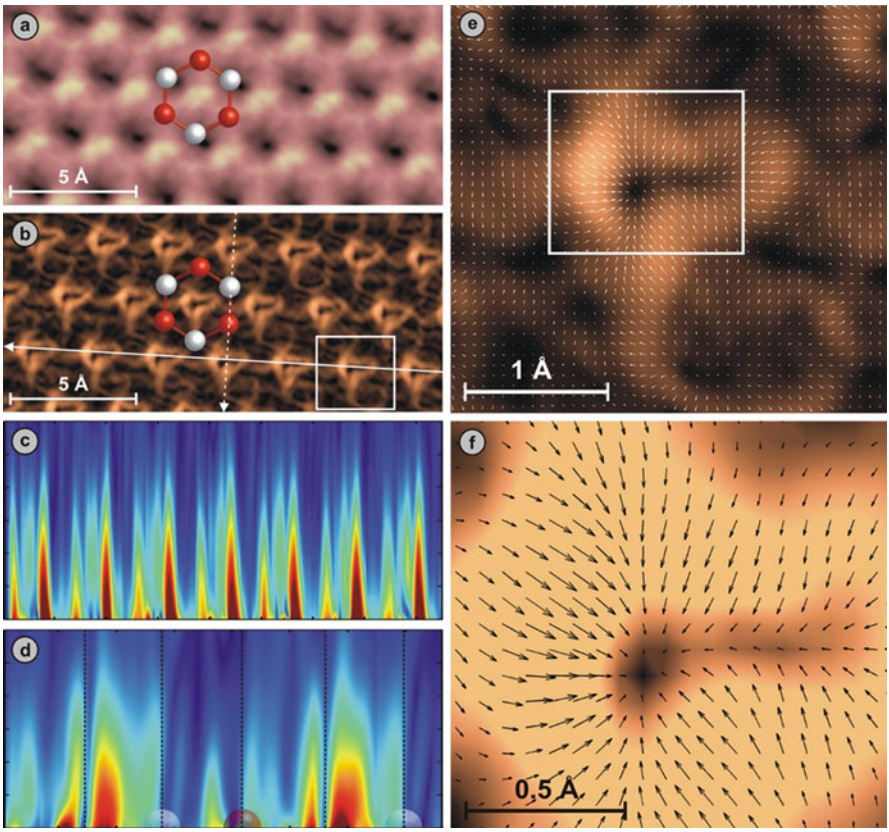

Fig. 8.15 Horizontal maps of normal (**a**) and lateral (**b**) interaction forces above the HOPG surface. The color scale in (**b**) ranges from 0 to 120 pN. Note the localization of lateral forces around the hollow sites of the HOPG lattice. (**c**) and (**d**) visualize the evolution of lateral forces as a function of tip-sample distance along the *straight* and *dashed arrows* in (**b**) while (**e**) and (**f**) describe in very high resolution the distribution of lateral force vectors around the hollow sites (Figure reproduced from Ref. [85] © IOP Publishing. Reproduced with permission. All rights reserved)

where depicted vectors (separated by ∼7 pm) indicate the direction and magnitude of the measured lateral force at each data point. The authors have argued that this remarkable localization of lateral forces might help explain the exceptional frictional properties of HOPG as a solid lubricant [84, 85].

Additionally, using vertical cuts of lateral forces along crystallographic directions of interest, it is shown that atomic-scale corrugation in terms of lateral forces disappears at about 120 pm above the plane of closest approach (corresponding to a vertical force magnitude of about 1.6 nN) and the maximum lateral force detected in the bottom plane is ∼0.2 nN, a comparable value to some of the previously published results on KBr [81] and Si [82].

After atomic-resolution force spectroscopy in three dimensions has been demonstrated as a proof of principle on the model surface of HOPG [84], several other

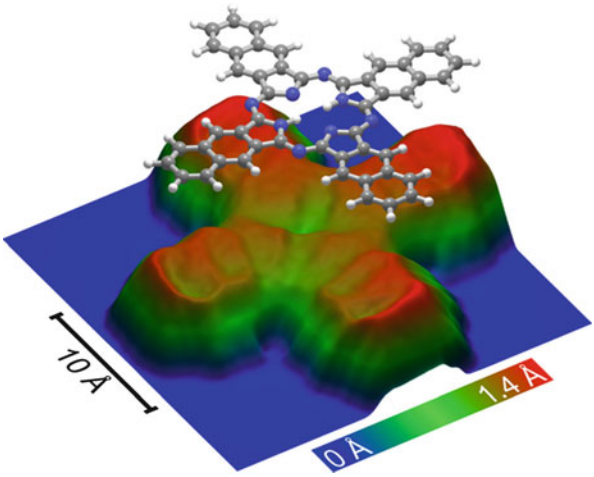

Fig. 8.16 A three-dimensional representation of the topography associated with a single naphthalocyanine molecule at constant tip-sample interaction. The data has been extracted from a full three-dimensional set of frequency shifts utilized for force spectroscopy (Figure reproduced from Ref. [110]. Copyright (2011), AIP Publishing LLC)

experiments have shown the feasibility of the technique on other sample systems. Specifically, in a groundbreaking experiment, Gross et al. have been able to image the intramolecular structure of a pentacene molecule using a tip apex functionalized with a CO molecule, whereby they have also performed three-dimensional force spectroscopy [61]. Again using a CO-modified tip apex, Mohn et al. have measured the three-dimensional short-range force field over a naphthalocyanine molecule (Fig. 8.16) [110]. Moreover Such et al. have utilized the technique to show that significant tip relaxation based on changing tip-sample distance is observable for specific tip apices during spectroscopy experiments [111] and that a height-dependent contrast reversal occurs during spectroscopy experiments on Cu(111) [112]. Fremy et al. have compared the advantages and disadvantages of the *curve-by-curve* and *layer-by-layer* data acquisition methods for three-dimensional force spectroscopy on a model ionic crystal surface (KBr) [87], while Kawai et al. have studied interaction induced atomic relaxations [107] and Sugimoto et al. have simultaneously performed three-dimensional force and tunneling current spectroscopy on Si(111)-7×7 [108]. Furthermore, using three-dimensional force spectroscopy, Pawlak et al. have investigated the mechanical properties of C_{60} molecules [225] as well porphyrin derivatives [228]. It is important to note that a significant number of three-dimensional spectroscopy experiments mentioned here have been performed at room temperature thanks to the use of atom-tracking/feedforward methods [87, 107, 108]. Finally, Giessibl et al. have performed a combined three-dimensional study of interaction forces and tunneling current on a single CO molecule adsorbed on a copper surface, whereby they were able to observe angular dependence of measured chemical interaction forces on changing crystallographic orientation of a tungsten tip apex [249]. While all force spectroscopy experiments mentioned here have been performed under UHV conditions, attention should be drawn to the fact that the technique has recently been extended to liquid conditions thanks to certain

developments in instrumentation and methodology, an important step towards broadening the application areas of NC-AFM based spectroscopy experiments [128, 129, 250, 251].

5.2.3 Combined Three-Dimensional Force and Tunneling Current Spectroscopy with Atomic Resolution

One of the important advantages associated with the three-dimensional force spectroscopy technique performed via NC-AFM is that additional data channels such as dissipated energy and tunneling current may be recorded during the experiments [22]. Simultaneous recording of interaction forces and tunneling currents is of particular interest due to the fact that information about atomic-scale chemical interactions exhibited by surface atoms with the tip apex and at the same time, clues regarding the electronic properties of the surface are collected concurrently such that the data in the two channels can be contrasted and compared. Moreover, the complementary information included in the two channels can be used towards identification of lattice sites on sample surfaces consisting of more than one type of atom where symmetry arguments in a single channel do not allow for an unambiguous assignment of lattice sites to observed maxima. Additionally, chemical and structural identification of the tip apex used in specific experiments remains a significant issue, which can be facilitated by the additional data available in the tunneling current channel, especially if the experimental data is interpreted with help from ab initio simulations.

To illustrate the points described above, a simultaneously recorded data set of interaction forces and tunneling currents on a surface-oxidized Cu(100) sample will be presented as a representative example [86] (keeping in mind that other studies exist where combined three-dimensional force and tunneling current spectroscopy have been performed, as well [108, 249]). The monolayer-thick surface oxide layer investigated in the experiments described here features a missing-row reconstruction where one in every four copper rows of the underlying substrate forms a trough, with filled rows between the troughs consisting of nearly co-planar Cu and O atoms in an alternating configuration (Fig. 8.17a). The spectroscopy experiments have been performed using the same instrument [101] utilized for acquiring the pioneering three-dimensional force spectroscopy data on HOPG [84] at liquid helium temperatures and a quartz tuning fork in the *qPlus* configuration with an etched and field-ion beam treated Pt/Ir tip as the force sensor. While the tuning fork is oscillating with a an amplitude of $\sim$1.0 nm above the sample surface, frequency shift and tunneling current data (averaged over the oscillatory motion of the tip) are acquired *layer-by-layer* in a dense grid above the surface. After drift correction, the region of the surface over which the spectroscopy data is displayed remains 2.89 nm $\times$ 2.89 nm, featuring 221 $\times$ 221 pixels.

The three-dimensional map of interaction forces collected as described above is displayed in Fig. 8.17b, where the average force value at each height has been subtracted to enhance the contrast. The magnitude of the maximum interaction force measured in the bottom plane is $\sim$1.34 nN whereas the contrast between atomically defined lattice sites is $\sim$23 pN.

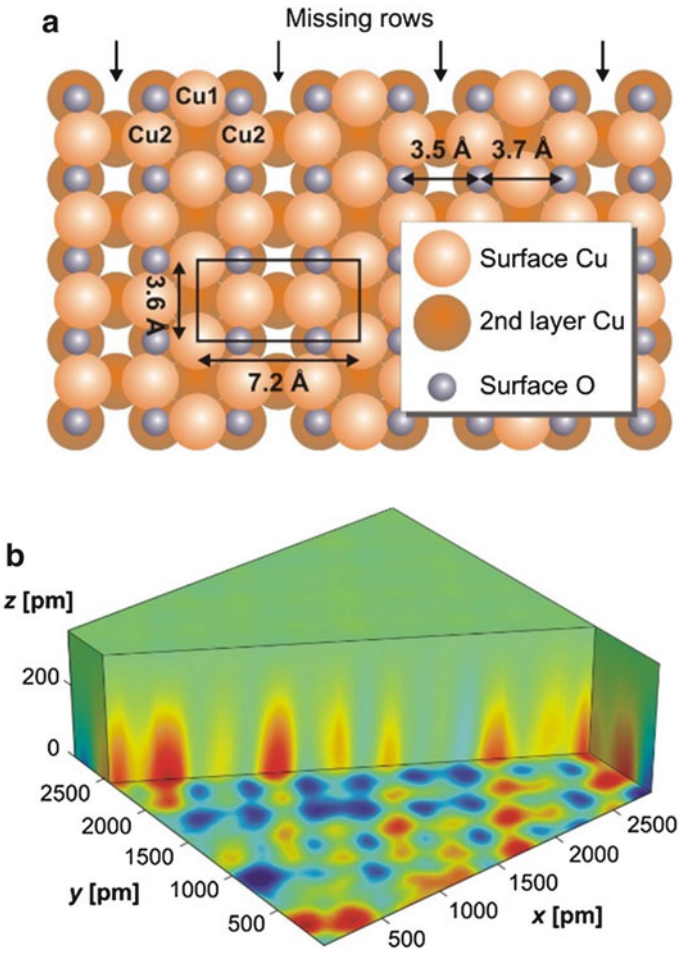

Fig. 8.17 (**a**) Reconstructed missing-row model of the surface oxide layer on Cu(100). Cu1 atoms are located at the centers of filled rows while Cu2 atoms are at the edges. (**b**) Three-dimensional representation of interaction forces obtained on the sample surface using NC-AFM based spectroscopy. Atomic corrugation is clearly observable on the plane of closest approach (Figure reproduced from Ref. [86]. Copyright (2013) by the American Physical Society)

Studying the atomic-scale arrangement of interaction forces on a *horizontal* cut produced from the three-dimensional map allows an unambiguous determination of force maxima as the O atoms on the surface (Fig. 8.18a), based on symmetry arguments. Interestingly, the interaction force observed on each O atom is different, with the values measured for each atom differing by as much as 40 % of the total force contrast at that distance. On the other hand, the corresponding tunneling current map obtained at the same fixed height features a *ladder-like* symmetry, with the occasional appearance of linear defects imaged as partially *nonmissing rows* (Fig. 8.18b). Comparison of the obtained experimental data with ab initio

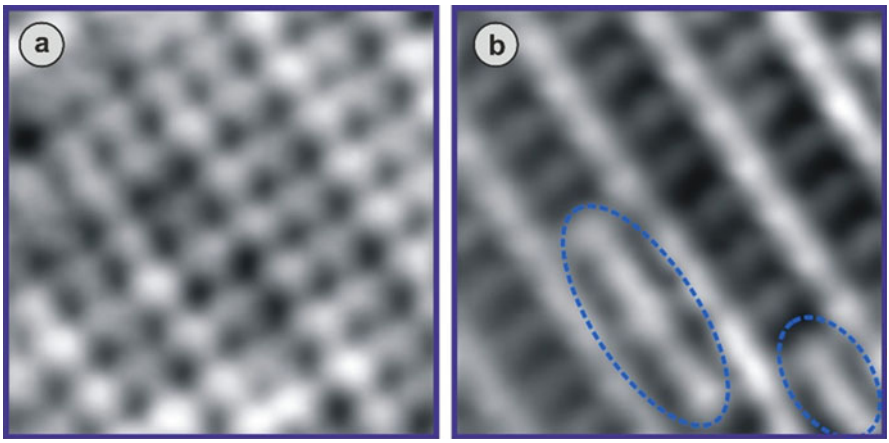

Fig. 8.18 (**a**) Horizontal force map (2.89 nm × 2.89 nm) extracted from the data in Fig. 8.17b at the plane of closest approach. Maxima are observed to coincide with the oxygen atoms on the surface. (**b**) Simultaneously acquired image of average tunneling current at the same height. A *ladder-type* contrast coinciding with the copper atom arrangement on the surface is observed, together with highlighted surface defects (Figure reproduced from Ref. [86]. Copyright (2013) by the American Physical Society)

density functional theory calculations involving model tip apices consisting of Cu and O atoms (selected due to the fact that tips have been treated by gentle crashes into the sample surface prior to data acquisition to improve imaging resolution) then allows to (a) identify the structure and chemistry of the tip apex used in the experiments by a comparison with simulated force curves and tunneling current images, and (b) identify the linear defects observed in the tunneling current channel. Consequently, the tip apex used in the experiments is predicted to be terminated by a Cu atom with an O atom adsorbed on the side, which successfully reproduces the experimentally obtained contrast in the tunneling current channel (where Cu1 atoms located at the centers of filled rows are imaged as bright protrusions and faint bridges of tunneling current are formed by Cu2 atoms on both sides of the missing rows) and interacts most favorably with the O atoms on the surface in the investigated height regime. Simultaneous imaging of two different chemical species via multichannel NC-AFM is thus demonstrated. Moreover, after investigating a number of defect models and the resulting simulations of tunneling current contrast, the atomic-scale origin of the linear defect observed in the current channel can be determined to involve the displacement of two pairs of Cu2 atoms into the missing rows (Fig. 8.19a, b). The authors eventually conclude that the variation of interaction force observed on each O atom is due to the variability in the chemical and electronic environment induced by the existence of surface defects, thereby providing a direct, real-space evidence that surface defects affect chemical reactivity on the atomic scale [86].

As seen by the representative example presented here, the combination of three-dimensional force and tunneling current spectroscopy performed via NC-AFM

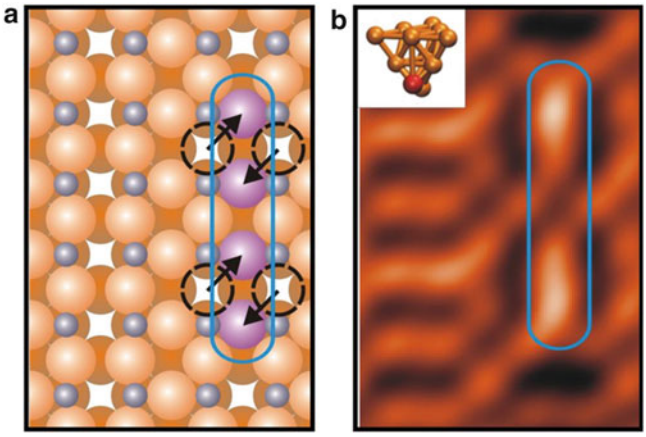

Fig. 8.19 A surface defect model involving the displacement of two pairs of Cu_2 atoms into the missing row (**a**) is predicted to result in the observation of a linear defect in the tunneling current channel (**b**) via ab initio simulations, in alignment with experimental data displayed in Fig. 8.18b. The *inset* in (**b**) represents the structural model of the tip apex used in the simulations (Figure reproduced from Ref. [86]. Copyright (2013) by the American Physical Society)

exhibits a tremendous potential for atomic-scale characterization of surfaces featuring multiple chemical species and even defects. As such, in addition to its atomic-resolution imaging capabilities, NC-AFM emerges as a very powerful tool for ultra-high resolution physical, chemical and mechanical characterization of material surfaces.

6 Conclusions and Outlook

The immense application potential of NC-AFM as an ultra-high resolution characterization tool for nanoscience and nanotechnology has been demonstrated by the results presented in this chapter. With NC-AFM, researchers now have the capability to characterize the structure of various material surfaces including semiconductors, metal oxides, ionic crystals, etc. with atomic resolution, while force spectroscopy experiments allow the site-specific quantification of chemical interactions, paving the way towards full atomic-scale characterization of surface reactivity – a topic of fundamental importance for numerous fields including tribology and heterogeneous catalysis.

While atomic-resolution NC-AFM experiments have been restricted to ultrahigh vacuum conditions for a long time, advances in instrumentation and experimental methodology now allow molecular- and atomic-resolution imaging studies to be performed in ambient conditions as well as liquids. As such, it is expected that the application of NC-AFM will expand in the near future towards high resolution characterization of different types of functional biological materials under liquid environment, where the structural integrity of investigated molecules and molecular structures are conserved.

As demonstrated throughout the chapter via numerous experimental and theoretical studies, results obtained by NC-AFM strongly depend on the structural and chemical properties of the tip apex. While tip apex standardization has been reached to some extent via functionalization through adsorbed molecules such as CO, the next step in this direction could involve the functionalization of tip apices via molecules that are of particular importance with regards to certain applications such as catalysis. Within this context, the ability to fully map the potential energy landscape experienced by particular molecules in the vicinity of single crystal substrates of catalytic importance would result in the acquisition of much needed data in terms of the effect of defects (such as step edges, kinks as well as vacancies, etc.) on site-specific chemical reactivity.

Last but not least, the demonstrated capability of the method to simultaneously acquire structural, physical, chemical as well as electronic information regarding material surfaces on the atomic scale via the recording of multiple data channels holds great potential for future applications of nanotechnology. Combined with the fact that NC-AFM can now be used to perform atomic manipulation experiments on surfaces [252, 253], the vision of true bottom-up engineering on the nanoscale involving the rational construction and subsequent characterization of atomic-scale, functional structures may be realized in the near future.

References

1. Binnig G, Rohrer H (1982) Scanning tunneling microscopy. Helv Phys Acta 55(6):726–735
2. Binnig G, Rohrer H, Gerber C, Weibel E (1983) 7x7 Reconstruction on Si(111) resolved in real space. Phys Rev Lett 50(2):120–123
3. Chen CJ (2007) Introduction to scanning tunneling microscopy. Oxford University Press, Oxford
4. Bonnell DA, Basov DN, Bode M, Diebold U, Kalinin SV, Madhavan V, Novotny L, Salmeron M, Schwarz UD, Weiss PS (2012) Imaging physical phenomena with local probes: from electrons to photons. Rev Mod Phys 84(3):1343
5. Binnig G, Quate CF, Gerber C (1986) Atomic force microscope. Phys Rev Lett 56(9):930–933
6. Albrecht TR, Quate CF (1988) Atomic resolution with the atomic force microscope on conductors and nonconductors. J Vac Sci Technol Vac Surf Films 6(2):271–274
7. Albrecht TR, Akamine S, Carver TE, Quate CF (1990) Microfabrication of cantilever styli for the atomic force microscope. J Vac Sci Technol-Vac Surf Films 8(4):3386–3396
8. Akamine S, Barrett RC, Quate CF (1990) Improved atomic force microscope images using microcantilevers with sharp tips. Appl Phys Lett 57(3):316–318
9. Wolter O, Bayer T, Greschner J (1991) Micromachined silicon sensors for scanning force microscopy. J Vac Sci Technol B 9(2):1353–1357
10. Meyer G, Amer NM (1988) Novel optical approach to atomic force microscopy. Appl Phys Lett 53(12):1045–1047
11. Alexander S, Hellemans L, Marti O, Schneir J, Elings V, Hansma PK, Longmire M, Gurley J (1989) An atomic-resolution atomic-force microscope implemented using an optical-lever. J Appl Phys 65(1):164–167
12. Rugar D, Mamin HJ, Guethner P (1989) Improved fiber-optic interferometer for atomic force microscopy. Appl Phys Lett 55(25):2588–2590
13. Moser A, Hug HJ, Jung T, Schwarz UD, Guntherodt HJ (1993) A miniature fiber optic force microscope scan head. Meas Sci Technol 4(7):769–775

14. Binnig G, Gerber C, Stoll E, Albrecht TR, Quate CF (1987) Atomic resolution with atomic force microscope. Europhys Lett 3(12):1281–1286
15. Meyer G, Amer NM (1990) Optical-beam-deflection atomic force microscopy – the nacl (001) surface. Appl Phys Lett 56(21):2100–2101
16. Marti O, Colchero J, Mlynek J (1993) Friction and forces on an atomic-scale. Nanosour Manip Atoms Under High Fields Temp Appl 235:253–269
17. Meyer G, Amer NM (1990) Simultaneous measurement of lateral and normal forces with an optical-beam-deflection atomic force microscope. Appl Phys Lett 57(20):2089–2091
18. Mate CM, McClelland GM, Erlandsson R, Chiang S (1987) Atomic-scale friction of a tungsten tip on a graphite surface. Phys Rev Lett 59(17):1942–1945
19. Eaton PJ, West P (2010) Atomic force microscopy. Oxford University Press, Oxford
20. Giessibl FJ, Binnig G (1992) Investigation of the (001) cleavage plane of potassium-bromide with an atomic force microscope at 4.2-k in ultra-high vacuum. Ultramicroscopy 42:281–289
21. Ohnesorge F, Binnig G (1993) True atomic-resolution by atomic force microscopy through repulsive and attractive forces. Science 260(5113):1451–1456
22. Baykara MZ, Schwendemann TC, Altman EI, Schwarz UD (2010) Three-dimensional atomic force microscopy – taking surface imaging to the next level. Adv Mater 22(26–27):2838–2853
23. Giessibl FJ (1995) Atomic-resolution of the silicon (111)-(7x7) surface by atomic-force microscopy. Science 267(5194):68–71
24. Sugawara Y, Ohta M, Ueyama H, Morita S (1995) Defect motion on an InP(110) surface observed with noncontact atomic-force microscopy. Science 270(5242):1646–1648
25. Kitamura S, Iwatsuki M (1995) Observation of 7x7 reconstructed structure on the silicon (111) surface using ultrahigh-vacuum noncontact atomic-force microscopy. Jpn J Appl Phys Part 2 Lett 34(1B):L145–L148
26. Ueyama H, Ohta M, Sugawara Y, Morita S (1995) Atomically resolved InP(110) surface observed with noncontact ultrahigh-vacuum atomic-force microscope. Jpn J Appl Phys Part 2 Lett 34(8B):L1086–L1088
27. Morita S, Wiesendanger R, Meyer E (2002) Noncontact atomic force microscopy. Springer, Berlin
28. Morita S, Giessibl FJ, Wiesendanger R (2009) Noncontact atomic force microscopy, vol 2. Springer, Berlin
29. Garcia R, Perez R (2002) Dynamic atomic force microscopy methods. Surf Sci Rep 47(6–8):197–301
30. Giessibl FJ (2003) Advances in atomic force microscopy. Rev Mod Phys 75(3):949–983
31. Hofer WA, Foster AS, Shluger AL (2003) Theories of scanning probe microscopes at the atomic scale. Rev Mod Phys 75(4):1287–1331
32. Barth C, Foster AS, Henry CR, Shluger AL (2011) Recent trends in surface characterization and chemistry with high-resolution scanning force methods. Adv Mater 23(4):477–501
33. Morita S (2013) Atomically resolved force microscopy. J Vac Sci Technol A 31(5):050802
34. Albrecht TR, Grutter P, Horne D, Rugar D (1991) Frequency-modulation detection using high-q cantilevers for enhanced force microscope sensitivity. J Appl Phys 69(2):668–673
35. Yokoyama K, Ochi T, Yoshimoto A, Sugawara Y, Morita S (2000) Atomic resolution imaging on Si(100)2x1 and Si(100)2x1: H surfaces with noncontact atomic force microscopy. Japanese J Appl Phys Part 2 Lett 39(2A):L113–L115
36. Schwarz A, Allers W, Schwarz UD, Wiesendanger R (2000) Dynamic-mode scanning force microscopy study of n-InAs(110)-(1x1) at low temperatures. Phys Rev B 61(4):2837–2845
37. Kitamura S, Iwatsuki M (1996) Observation of silicon surfaces using ultrahigh-vacuum noncontact, atomic force microscopy. Jpn J Appl Phys Part 2-Lett 35(5B):L668–L671
38. Sugawara Y, Uchihashi T, Abe M, Morita S (1999) True atomic resolution imaging of surface structure and surface charge on the GaAs(110). Appl Surf Sci 140(3–4):371–375
39. Sawada D, Sugimoto Y, Morita K, Abe M, Morita S (2010) Simultaneous atomic force and scanning tunneling microscopy study of the Ge(111)-c(2x8) surface. J Vac Sci Technol B 28(3):C4D1

40. Yokoyama K, Ochi T, Sugawara Y, Morita S (1999) Atomically resolved silver imaging on the Si(111)-$\left(\sqrt{3} \times \sqrt{3}\right)$-Ag surface using a noncontact atomic force microscope. Phys Rev Lett 83(24):5023–5026
41. Sweetman A, Gangopadhyay S, Danza R, Berdunov N, Moriarty P (2009) qPlus atomic force microscopy of the Si(100) surface: buckled, split-off, and added dimers. Appl Phys Lett 95(6):063112
42. Sweetman A, Danza R, Gangopadhyay S, Moriarty P (2012) Imaging and manipulation of the Si(100) surface by small-amplitude NC-AFM at zero and very low applied bias. J Phys Condens Matter 24(8):084009
43. Sweetman A, Stannard A, Sugimoto Y, Abe M, Morita S, Moriarty P (2013) Simultaneous noncontact AFM and STM of Ag:Si(111)-$\left(\sqrt{3} \times \sqrt{3}\right)$R30°. Phys Rev B 87(7):075310
44. Li YJ, Nomura H, Ozaki N, Naitoh Y, Kageshima M, Sugawara Y, Hobbs C, Kantorovich L (2006) Origin of p(2 x 1) phase on Si(001) by noncontact atomic force microscopy at 5 k. Phys Rev Lett 96(10):106104
45. Naitoh Y, Ma ZM, Li YJ, Kageshima M, Sugawara Y (2010) Simultaneous observation of surface topography and elasticity at atomic scale by multifrequency frequency modulation atomic force microscopy. J Vac Sci Technol B 28(6):1210–1214
46. Minobe T, Uchihashi T, Tsukamoto T, Orisaka S, Sugawara Y, Morita S (1999) Distance dependence of noncontact-AFM image contrast on Si(111)$\sqrt{3} \times \sqrt{3}$-Ag structure. Appl Surf Sci 140(3–4):298–303
47. Orisaka S, Minobe T, Uchihashi T, Sugawara Y, Morita S (1999) The atomic resolution imaging of metallic Ag(111) surface by noncontact atomic force microscope. Appl Surf Sci 140(3–4):243–246
48. Loppacher C, Bammerlin M, Guggisberg M, Schar S, Bennewitz R, Baratoff A, Meyer E, Guntherodt HJ (2000) Dynamic force microscopy of copper surfaces: atomic resolution and distance dependence of tip-sample interaction and tunneling current. Phys Rev B 62(24):16944–16949
49. Caciuc V, Holscher H, Weiner D, Fuchs H, Schirmeisen A (2008) Noncontact atomic force microscopy imaging mechanism on Ag(110): experiment and first-principles theory. Phys Rev B 77(4):045411
50. Konig T, Simon GH, Rust HP, Heyde M (2009) Atomic resolution on a metal single crystal with dynamic force microscopy. Appl Phys Lett 95(8):083116
51. Allers W, Schwarz A, Schwarz UD, Wiesendanger R (1999) Dynamic scanning force microscopy at low temperatures on a noble-gas crystal: atomic resolution on the xenon (111) surface. Europhys Lett 48(3):276–279
52. Barth C, Reichling M (2001) Imaging the atomic arrangements on the high-temperature reconstructed alpha-Al_2O_3(0001) surface. Nature 414(6859):54–57
53. Reichling M, Barth C (1999) Scanning force imaging of atomic size defects on the CaF_2(111) surface. Phys Rev Lett 83(4):768–771
54. Barth C, Foster AS, Reichling M, Shluger AL (2001) Contrast formation in atomic resolution scanning force microscopy on CaF(2)(111): experiment and theory. J Phys-Condens Matter 13(10):2061–2079
55. Hoffmann R, Lantz MA, Hug HJ, van Schendel PJA, Kappenberger P, Martin S, Baratoff A, Guntherodt HJ (2003) Atomic resolution imaging and frequency versus distance measurements on NiO(001) using low-temperature scanning force microscopy. Phys Rev B 67(8):085402
56. Ruschmeier K, Schirmeisen A, Hoffmann R (2009) Site-specific force-vector field studies of KBr(001) by atomic force microscopy. Nanotechnology 20(26):264013
57. Gritschneder S, Namai Y, Iwasawa Y, Reichling M (2005) Structural features of CeO_2(111) revealed by dynamic SFM. Nanotechnology 16(3):S41–S48
58. Ostendorf F, Torbrugge S, Reichling M (2008) Atomic scale evidence for faceting stabilization of a polar oxide surface. Phys Rev B 77(4):041405
59. Rasmussen MK, Foster AS, Canova FF, Hinnemann B, Helveg S, Meinander K, Besenbacher F, Lauritsen JV (2011) Noncontact atomic force microscopy imaging of atomic

structure and cation defects of the polar $MgAl_2O_4(100)$ surface: experiments and first-principles simulations. Phys Rev B 84(23):235419
60. Hoffmann R, Weiner D, Schirmeisen A, Foster AS (2009) Sublattice identification in noncontact atomic force microscopy of the NaCl(001) surface. Phys Rev B 80(11):115426
61. Gross L, Mohn F, Moll N, Liljeroth P, Meyer G (2009) The chemical structure of a molecule resolved by atomic force microscopy. Science 325(5944):1110–1114
62. Gross L, Mohn F, Moll N, Meyer G, Ebel R, Abdel-Mageed WM, Jaspars M (2010) Organic structure determination using atomic-resolution scanning probe microscopy. Nat Chem 2(10):821–825
63. Meyer G, Gross L, Mahn F, Repp J (2012) Scanning probe microscopy of atoms and molecules on insulating films: from imaging to molecular manipulation. Chimia 66(1–2):10–15
64. Mohn F, Schuler B, Gross L, Meyer G (2013) Different tips for high-resolution atomic force microscopy and scanning tunneling microscopy of single molecules. Appl Phys Lett 102(7):073109
65. Gotsmann B, Anczykowski B, Seidel C, Fuchs H (1999) Determination of tip-sample interaction forces from measured dynamic force spectroscopy curves. Appl Surf Sci 140(3–4):314–319
66. Durig U (1999) Relations between interaction force and frequency shift in large-amplitude dynamic force microscopy. Appl Phys Lett 75(3):433–435
67. Giessibl FJ (2001) A direct method to calculate tip-sample forces from frequency shifts in frequency-modulation atomic force microscopy. Appl Phys Lett 78(1):123–125
68. Sader JE, Jarvis SP (2004) Accurate formulas for interaction force and energy in frequency modulation force spectroscopy. Appl Phys Lett 84(10):1801–1803
69. Giessibl FJ (1997) Forces and frequency shifts in atomic-resolution dynamic-force microscopy. Phys Rev B 56(24):16010–16015
70. Durig U (2000) Extracting interaction forces and complementary observables in dynamic probe microscopy. Appl Phys Lett 76(9):1203–1205
71. Holscher H, Schwarz A, Allers W, Schwarz UD, Wiesendanger R (2000) Quantitative analysis of dynamic-force-spectroscopy data on graphite(0001) in the contact and noncontact regimes. Phys Rev B 61(19):12678–12681
72. Gotsmann B, Fuchs H (2001) Dynamic force spectroscopy of conservative and dissipative forces in an Al-Au(111) tip-sample system. Phys Rev Lett 86(12):2597–2600
73. Lantz MA, Hug HJ, Hoffmann R, van Schendel PJA, Kappenberger P, Martin S, Baratoff A, Guntherodt HJ (2001) Quantitative measurement of short-range chemical bonding forces. Science 291(5513):2580–2583
74. Hoffmann R, Kantorovich LN, Baratoff A, Hug HJ, Guntherodt HJ (2004) Sublattice identification in scanning force microscopy on alkali halide surfaces. Phys Rev Lett 92(14):146103
75. Abe M, Sugimoto Y, Custance O, Morita S (2005) Room-temperature reproducible spatial force spectroscopy using atom-tracking technique. Appl Phys Lett 87(17):173503
76. Sugimoto Y, Innami S, Abe M, Custance O, Morita S (2007) Dynamic force spectroscopy using cantilever higher flexural modes. Appl Phys Lett 91(9):093120
77. Sugimoto Y, Pou P, Abe M, Jelinek P, Perez R, Morita S, Custance O (2007) Chemical identification of individual surface atoms by atomic force microscopy. Nature 446(7131):64–67
78. Langkat SM, Holscher H, Schwarz A, Wiesendanger R (2003) Determination of site specific interatomic forces between an iron coated tip and the NiO(001) surface by force field spectroscopy. Surf Sci 527(1–3):12–20
79. Schirmeisen A, Weiner D, Fuchs H (2006) Single-atom contact mechanics: from atomic scale energy barrier to mechanical relaxation hysteresis. Phys Rev Lett 97(13):136101
80. Heyde M, Simon GH, Rust HP, Freund HJ (2006) Probing adsorption sites on thin oxide films by dynamic force microscopy. Appl Phys Lett 89(26):263107

81. Ruschmeier K, Schirmeisen A, Hoffmann R (2008) Atomic-scale force-vector fields. Phys Rev Lett 101(15):156102
82. Sugimoto Y, Namikawa T, Miki K, Abe M, Morita S (2008) Vertical and lateral force mapping on the Si(111)-(7x7) surface by dynamic force microscopy. Phys Rev B 77(19):195424
83. Ashino M, Obergfell D, Haluska M, Yang SH, Khlobystov AN, Roth S, Wiesendanger R (2008) Atomically resolved mechanical response of individual metallofullerene molecules confined inside carbon nanotubes. Nat Nanotechnol 3(6):337–341
84. Albers BJ, Schwendemann TC, Baykara MZ, Pilet N, Liebmann M, Altman EI, Schwarz UD (2009) Three-dimensional imaging of short-range chemical forces with picometre resolution. Nat Nanotechnol 4(5):307–310
85. Baykara MZ, Schwendemann TC, Albers BJ, Pilet N, Monig H, Altman EI, Schwarz UD (2012) Exploring atomic-scale lateral forces in the attractive regime: a case study on graphite (0001). Nanotechnology 23(40):405703
86. Baykara MZ, Todorovic M, Monig H, Schwendemann TC, Unverdi O, Rodrigo L, Altman EI, Perez R, Schwarz UD (2013) Atom-specific forces and defect identification on surface-oxidized Cu(100) with combined 3D-AFM and STM measurements. Phys Rev B 87(15):155414
87. Fremy S, Kawai S, Pawlak R, Glatzel T, Baratoff A, Meyer E (2012) Three-dimensional dynamic force spectroscopy measurements on KBr(001): atomic deformations at small tip-sample separations. Nanotechnology 23(5):055401
88. Baykara MZ, Dagdeviren OE, Schwendemann TC, Monig H, Altman EI, Schwarz UD (2012) Probing three-dimensional surface force fields with atomic resolution: measurement strategies, limitations, and artifact reduction. Beilstein J Nanotechnol 3:637–650
89. Pethica JB (1986) Interatomic forces in scanning tunneling microscopy – giant corrugations of the graphite surface – comment. Phys Rev Lett 57(25):3235
90. Martin Y, Williams CC, Wickramasinghe HK (1987) Atomic force microscope force mapping and profiling on a sub 100-a scale. J Appl Phys 61(10):4723–4729
91. Zhong Q, Inniss D, Kjoller K, Elings VB (1993) Fractured polymer silica fiber surface studied by tapping mode atomic-force microscopy. Surf Sci 290(1–2):L688–L692
92. Castro García R (2010) Amplitude modulation atomic force microscopy. Wiley-VCH, Weinheim
93. Erlandsson R, Olsson L, Martensson P (1996) Inequivalent atoms and imaging mechanisms in ac-mode atomic-force microscopy of Si(111)7x7. Phys Rev B 54(12):R8309–R8312
94. Israelachvili JN (2011) Intermolecular and surface forces. Academic, Burlington
95. Moll N, Gross L, Mohn F, Curioni A, Meyer G (2010) The mechanisms underlying the enhanced resolution of atomic force microscopy with functionalized tips. New J Phys 12(12):125020
96. Fukui K, Onishi H, Iwasawa Y (1997) Atom-resolved image of the TiO_2(110) surface by noncontact atomic force microscopy. Phys Rev Lett 79(21):4202–4205
97. Allers W, Schwarz A, Schwarz UD, Wiesendanger R (1999) Dynamic scanning force microscopy at low temperatures on a van der Waals surface: graphite (0001). Appl Surf Sci 140(3–4):247–252
98. Giessibl FJ (2000) Atomic resolution on Si(111)-(7x7) by noncontact atomic force microscopy with a force sensor based on a quartz tuning fork. Appl Phys Lett 76(11):1470–1472
99. Giessibl FJ, Hembacher S, Bielefeldt H, Mannhart J (2000) Subatomic features on the silicon (111)-(7x7) surface observed by atomic force microscopy. Science 289(5478):422–425
100. Giessibl FJ, Hembacher S, Herz M, Schiller C, Mannhart J (2004) Stability considerations and implementation of cantilevers allowing dynamic force microscopy with optimal resolution: the qPlus sensor. Nanotechnology 15(2):S79–S86
101. Albers BJ, Liebmann M, Schwendemann TC, Baykara MZ, Heyde M, Salmeron M, Altman EI, Schwarz UD (2008) Combined low-temperature scanning tunneling/atomic force microscope for atomic resolution imaging and site-specific force spectroscopy. Rev Sci Instrum 79(3):033704

102. Giessibl FJ, Bielefeldt H, Hembacher S, Mannhart J (1999) Calculation of the optimal imaging parameters for frequency modulation atomic force microscopy. Appl Surf Sci 140(3–4):352–357
103. Perez R, Payne MC, Stich I, Terakura K (1997) Role of covalent tip-surface interactions in noncontact atomic force microscopy on reactive surfaces. Phys Rev Lett 78(4):678–681
104. Perez R, Stich I, Payne MC, Terakura K (1998) Surface-tip interactions in noncontact atomic-force microscopy on reactive surfaces: Si(111). Phys Rev B 58(16):10835–10849
105. Bennewitz R, Bammerlin M, Guggisberg M, Loppacher C, Baratoff A, Meyer E, Guntherodt HJ (1999) Aspects of dynamic force microscopy on NaCl/Cu(111): resolution, tip-sample interactions and cantilever oscillation characteristics. Surf Interface Anal 27(5–6):462–466
106. Guggisberg M, Bammerlin M, Loppacher C, Pfeiffer O, Abdurixit A, Barwich V, Bennewitz R, Baratoff A, Meyer E, Guntherodt HJ (2000) Separation of interactions by noncontact force microscopy. Phys Rev B 61(16):11151–11155
107. Kawai S, Glatzel T, Koch S, Baratoff A, Meyer E (2011) Interaction-induced atomic displacements revealed by drift-corrected dynamic force spectroscopy. Phys Rev B 83(3):035421
108. Sugimoto Y, Ueda K, Abe M, Morita S (2012) Three-dimensional scanning force/tunneling spectroscopy at room temperature. J Phys Condens Matter 24(8):084008
109. Braun DA, Weiner D, Such B, Fuchs H, Schirmeisen A (2009) Submolecular features of epitaxially grown PTCDA on Cu(111) analyzed by force field spectroscopy. Nanotechnology 20(26):264004
110. Mohn F, Gross L, Meyer G (2011) Measuring the short-range force field above a single molecule with atomic resolution. Appl Phys Lett 99(5):053106
111. Such B, Glatzel T, Kawai S, Koch S, Meyer E (2010) Three-dimensional force spectroscopy of KBr(001) by tuning fork-based cryogenic noncontact atomic force microscopy. J Vac Sci Technol B 28(3):C4B1
112. Such B, Glatzel T, Kawai S, Meyer E, Turansky R, Brndiar J, Stich I (2012) Interplay of the tip-sample junction stability and image contrast reversal on a Cu(111) surface revealed by the 3D force field. Nanotechnology 23(4):045705
113. Abe M, Sugimoto Y, Custance O, Morita S (2005) Atom tracking for reproducible force spectroscopy at room temperature with non-contact atomic force microscopy. Nanotechnology 16(12):3029–3034
114. Abe M, Sugimoto Y, Namikawa T, Morita K, Oyabu N, Morita S (2007) Drift-compensated data acquisition performed at room temperature with frequency modulation atomic force microscopy. Appl Phys Lett 90(20):203103
115. Enevoldsen GH, Pinto HP, Foster AS, Jensen MCR, Kuhnle A, Reichling M, Hofer WA, Lauritsen JV, Besenbacher F (2008) Detailed scanning probe microscopy tip models determined from simultaneous atom-resolved AFM and STM studies of the TiO(2)(110) surface. Phys Rev B 78(4):045416
116. Oyabu N, Pou P, Sugimoto Y, Jelinek P, Abe M, Morita S, Perez R, Custance O (2006) Single atomic contact adhesion and dissipation in dynamic force microscopy. Phys Rev Lett 96(10):106101
117. Pou P, Ghasemi SA, Jelinek P, Lenosky T, Goedecker S, Perez R (2009) Structure and stability of semiconductor tip apexes for atomic force microscopy. Nanotechnology 20(26):264015
118. Bechstein R, Gonzalez C, Schutte J, Jelinek P, Perez R, Kuhnle A (2009) 'All-inclusive' imaging of the rutile TiO_2(110) surface using NC-AFM. Nanotechnology 20(50):505703
119. Arai T, Gritschneder S, Troger L, Reichling M (2010) Atomic resolution force microscopy imaging on a strongly ionic surface with differently functionalized tips. J Vac Sci Technol B 28(6):1279–1283
120. Lauritsen JV, Foster AS, Olesen GH, Christensen MC, Kuhnle A, Helveg S, Rostrup-Nielsen JR, Clausen BS, Reichling M, Besenbacher F (2006) Chemical identification of point defects and adsorbates on a metal oxide surface by atomic force microscopy. Nanotechnology 17(14):3436–3441

121. Enevoldsen GH, Foster AS, Christensen MC, Lauritsen JV, Besenbacher F (2007) Noncontact atomic force microscopy studies of vacancies and hydroxyls of TiO(2)(110): experiments and atomistic simulations. Phys Rev B 76(20):205415
122. Uluutku B, Baykara MZ (2013) Effect of lateral tip stiffness on atomic-resolution force field spectroscopy. J Vac Sci Technol B 31(4):041801
123. Sun ZX, Boneschanscher MP, Swart I, Vanmaekelbergh D, Liljeroth P (2011) Quantitative atomic force microscopy with carbon monoxide terminated tips. Phys Rev Lett 106(4):046104
124. Schwarz A, Schwarz UD, Langkat S, Holscher H, Allers W, Wiesendanger R (2002) Dynamic force microscopy with atomic resolution at low temperatures. Appl Surf Sci 188(3–4):245–251
125. Rahe P, Schutte J, Schniederberend W, Reichling M, Abe M, Sugimoto Y, Kuhnle A (2011) Flexible drift-compensation system for precise 3D force mapping in severe drift environments. Rev Sci Instrum 82(6):063704
126. Fukuma T, Ichii T, Kobayashi K, Yamada H, Matsushige K (2005) True-molecular resolution imaging by frequency modulation atomic force microscopy in various environments. Appl Phys Lett 86(3):034103
127. Fukuma T, Kobayashi K, Matsushige K, Yamada H (2005) True atomic resolution in liquid by frequency-modulation atomic force microscopy. Appl Phys Lett 87(3):034101
128. Fukuma T, Ueda Y, Yoshioka S, Asakawa H (2010) Atomic-scale distribution of water molecules at the mica-water interface visualized by three-dimensional scanning force microscopy. Phys Rev Lett 104(1):016101
129. Herruzo ET, Asakawa H, Fukuma T, Garcia R (2013) Three-dimensional quantitative force maps in liquid with 10 piconewton, angstrom and sub-minute resolutions. Nanoscale 5(7):2678–2685
130. Asakawa H, Fukuma T (2009) Spurious-free cantilever excitation in liquid by piezoactuator with flexure drive mechanism. Rev Sci Instrum 80(10):103703
131. Asakawa H, Fukuma T (2009) The molecular-scale arrangement and mechanical strength of phospholipid/cholesterol mixed bilayers investigated by frequency modulation atomic force microscopy in liquid. Nanotechnology 20(26):264008
132. Mitani Y, Kubo M, Muramoto K, Fukuma T (2009) Wideband digital frequency detector with subtraction-based phase comparator for frequency modulation atomic force microscopy. Rev Sci Instrum 80(8):083705
133. Fukuma T (2009) Wideband low-noise optical beam deflection sensor with photothermal excitation for liquid-environment atomic force microscopy. Rev Sci Instrum 80(2):023707
134. Guthner P (1996) Simultaneous imaging of Si(111) 7x7 with atomic resolution in scanning tunneling microscopy, atomic force microscopy, and atomic force microscopy noncontact mode. J Vac Sci Technol B 14(4):2428–2431
135. Luthi R, Meyer E, Bammerlin M, Baratoff A, Lehmann T, Howald L, Gerber C, Guntherodt HJ (1996) Atomic resolution in dynamic force microscopy across steps on Si(111)7x7. Z Physik B-Condens Matter 100(2):165–167
136. Nakagiri N, Suzuki M, Okiguchi K, Sugimura H (1997) Site discrimination of adatoms in Si (111)-7x7 by noncontact atomic force microscopy. Surf Sci 373(1):L329–L332
137. Sawada D, Sugimoto Y, Abe M, Morita S (2010) Observation of subsurface atoms of the si (111)-(7x7) surface by atomic force microscopy. Appl Phys Express 3(11):116602
138. Sugimoto Y, Nakajima Y, Sawada D, Morita K, Abe M, Morita S (2010) Simultaneous AFM and STM measurements on the Si(111)-(7x7) surface. Phys Rev B 81(24):245322
139. Uozumi T, Tomiyoshi Y, Suehira N, Sugawara Y, Morita S (2002) Observation of Si(100) surface with noncontact atomic force microscope at 5 K. Appl Surf Sci 188(3–4):279–284
140. Sweetman A, Jarvis S, Danza R, Bamidele J, Gangopadhyay S, Shaw GA, Kantorovich L, Moriarty P (2011) Toggling bistable atoms via mechanical switching of bond angle. Phys Rev Lett 106(13):136101

141. Sweetman A, Jarvis S, Danza R, Bamidele J, Kantorovich L, Moriarty P (2011) Manipulating Si(100) at 5 K using qPlus frequency modulated atomic force microscopy: role of defects and dynamics in the mechanical switching of atoms. Phys Rev B 84(8):085426
142. Sweetman A, Jarvis S, Danza R, Moriarty P (2012) Effect of the tip state during qPlus noncontact atomic force microscopy of Si(100) at 5 K: probing the probe. Beilstein J Nanotechnol 3:25–32
143. Naitoh Y, Li YJ, Nomura H, Kageshima M, Sugawara Y (2010) Effect of surface stress around the sa step of Si(001) on the dimer structure determined by noncontact atomic force microscopy at 5 K. J Physical Soc Japan 79(1):013601
144. Sugimoto Y, Abe M, Yoshimoto K, Custance O, Yi I, Morita S (2005) Non-contact atomic force microscopy study of the Sn/Si(111) mosaic phase. Appl Surf Sci 241(1–2):23–27
145. Yi I, Sugimoto Y, Nishi R, Morita S (2006) Study on topographic images of Sn/Si(111)-$\left(\sqrt{3}\times\sqrt{3}\right)$R30° surface by non-contact AFM. Surf Sci 600(17):3382–3387
146. Yi I, Nishi R, Sugimoto Y, Morita S (2007) Non-contact AFM observation of the $\left(\sqrt{3}\times\sqrt{3}\right)$ to (3x3) phase transition on Sn/Ge(111) and Sn/Si(111) surfaces. Appl Surf Sci 253(6):3072–3076
147. Sugimoto Y, Pou P, Custance O, Jelinek P, Morita S, Perez R, Abe M (2006) Real topography, atomic relaxations, and short-range chemical interactions in atomic force microscopy: the case of the alpha-Sn/Si(111)-$\left(\sqrt{3}\times\sqrt{3}\right)$R30° surface. Phys Rev B 73(20):205329
148. Abe M, Sugimoto Y, Morita S (2005) Imaging the restatom of the Ge(111)-c(2x8) surface with noncontact atomic force microscopy at room temperature. Nanotechnology 16(3): S68–S72
149. Schwarz A, Allers W, Schwarz UD, Wiesendanger R (2000) Detection of doping atom distributions and individual dopants in InAs(110) by dynamic-mode scanning force microscopy in ultrahigh vacuum. Phys Rev B 62(20):13617–13622
150. Henrich VE, Cox PA (1994) The surface science of metal oxides. Cambridge University Press, Cambridge
151. Diebold U (2003) The surface science of titanium dioxide. Surf Sci Rep 48(5–8):53–229
152. Freund HJ, Pacchioni G (2008) Oxide ultra-thin films on metals: new materials for the design of supported metal catalysts. Chem Soc Rev 37(10):2224–2242
153. Raza H, Pang CL, Haycock SA, Thornton G (1999) Non-contact atomic force microscopy imaging of TiO_2(100) surfaces. Appl Surf Sci 140(3–4):271–275
154. Enevoldsen GH, Pinto HP, Foster AS, Jensen MCR, Hofer WA, Hammer B, Lauritsen JV, Besenbacher F (2009) Imaging of the hydrogen subsurface site in rutile TiO(2). Phys Rev Lett 102(13):136103
155. Yurtsever A, Sugimoto Y, Abe M, Morita S (2010) NC-AFM imaging of the TiO(2)(110)-(1x1) surface at low temperature. Nanotechnology 21(16):165702
156. Yurtsever A, Fernandez-Torre D, Gonzalez C, Jelinek P, Pou P, Sugimoto Y, Abe M, Perez R, Morita S (2012) Understanding image contrast formation in TiO_2 with force spectroscopy. Phys Rev B 85(12):125416
157. Pang CL, Raza H, Haycock SA, Thornton G (2002) Noncontact atomic force microscopy imaging of ultrathin Al_2O_3 on NiAl(110). Phys Rev B 65(20):201401
158. Wang J, Howard A, Egdell RG, Pethica JB, Foord JS (2002) Arrangement of rotational domains of the $\left(\sqrt{31}\times\sqrt{31}\right)$ R +/− 9° reconstruction of Al_2O_3(0001) revealed by non-contact AFM. Surf Sci 515(2–3):337–343
159. Simon GH, Konig T, Nilius M, Rust HP, Heyde M, Freund HJ (2008) Atomically resolved force microscopy images of complex surface unit cells: ultrathin alumina film on NiAl(110). Phys Rev B 78(11):113401
160. Simon GH, Konig T, Rust HP, Heyde M, Freund HJ (2009) Atomic structure of the ultrathin alumina on NiAl(110) and its antiphase domain boundaries as seen by frequency modulation dynamic force microscopy. New J Phys 11(9):093009

161. Lauritsen JV, Jensen MCR, Venkataramani K, Hinnemann B, Helveg S, Clausen BS, Besenbacher F (2009) Atomic-scale structure and stability of the $\left(\sqrt{31} \times \sqrt{31}\right)$R9° surface of Al_2O_3(0001). Phys Rev Lett 103(7):076103
162. Heyde M, Simon GH, Lichtenstein L (2013) Resolving oxide surfaces – from point and line defects to complex network structures. Phys Status Solidi B-Basic Solid State Phys 250(5):895–921
163. Simon GH, Konig T, Heinke L, Lichtenstein L, Heyde M, Freund HJ (2011) Atomic structure of surface defects in alumina studied by dynamic force microscopy: strain-relief-, translation- and reflection-related boundaries, including their junctions. New J Phys 13(12):123028
164. Fukui K, Namai Y, Iwasawa Y (2002) Imaging of surface oxygen atoms and their defect structures on CeO_2(111) by noncontact atomic force microscopy. Appl Surf Sci 188(3–4):252–256
165. Namai Y, Fukui KI, Iwasawa Y (2003) Atom-resolved noncontact atomic force microscopic and scanning tunneling microscopic observations of the structure and dynamic behavior of CeO_2(111) surfaces. Catal Today 85(2–4):79–91
166. Namai Y, Fukui K, Iwasawa Y (2003) Atom-resolved noncontact atomic force microscopic observations of CeO_2(111) surfaces with different oxidation states: surface structure and behavior of surface oxygen atoms. J Phys Chem B 107(42):11666–11673
167. Gritschneder S, Reichling M (2007) Structural elements of CeO_2(111) surfaces. Nanotechnology 18(4):044024
168. Gritschneder S, Reichling M (2008) Atomic resolution imaging on CeO_2(111) with hydroxylated probes. J Phys Chem C 112(6):2045–2049
169. Pieper HH, Derks C, Zoellner MH, Olbrich R, Troger L, Schroeder T, Neumann M, Reichling M (2012) Morphology and nanostructure of CeO_2(111) surfaces of single crystals and Si(111) supported ceria films. Phys Chem Chem Phys 14(44):15361–15368
170. Hosoi H, Sueoka K, Hayakawa K, Mukasa K (2000) Atomic resolved imaging of cleaved NiO(100) surfaces by NC-AFM. Appl Surf Sci 157(4):218–221
171. Allers W, Langkat S, Wiesendanger R (2001) Dynamic low-temperature scanning force microscopy on nickel oxide (001). Appl Phys Mater Sci Process 72:S27–S30
172. Kaiser U, Schwarz A, Wiesendanger R (2007) Magnetic exchange force microscopy with atomic resolution. Nature 446(7135):522–525
173. Schmid M, Mannhart J, Giessibl FJ (2008) Searching atomic spin contrast on nickel oxide (001) by force microscopy. Phys Rev B 77(4):045402
174. Kaiser U, Schwarz A, Wiesendanger R (2008) Evaluating local properties of magnetic tips utilizing an antiferromagnetic surface. Phys Rev B 78(10):104418
175. Barth C, Henry CR (2003) Atomic resolution imaging of the (001) surface of UHV cleaved MgO by dynamic scanning force microscopy. Phys Rev Lett 91(19):196102
176. Heyde M, Sterrer M, Rust HP, Freund HJ (2005) Atomic resolution on MgO(001) by atomic force microscopy using a double quartz tuning fork sensor at low-temperature and ultrahigh vacuum. Appl Phys Lett 87(8):083104
177. Heyde M, Sterrer M, Rust HP, Freund HJ (2006) Frequency modulated atomic force microscopy on MgO(001) thin films: interpretation of atomic image resolution and distance dependence of tip-sample interaction. Nanotechnology 17(7):S101–S106
178. Torbrugge S, Ostendorf F, Reichling M (2009) Stabilization of zinc-terminated ZnO(0001) by a modified surface stoichiometry. J Phys Chem C 113(12):4909–4914
179. Suzuki S, Ohminami Y, Tsutsumi T, Shoaib MM, Ichikawa M, Asakura K (2003) The first observation of an atomic scale noncontact AFM image of MoO_3(010). Chem Lett 32(12):1098–1099
180. Rasmussen MK, Foster AS, Hinnemann B, Canova FF, Helveg S, Meinander K, Martin NM, Knudsen J, Vlad A, Lundgren E, Stierle A, Besenbacher F, Lauritsen JV (2011) Stable cation inversion at the $MgAl_2O_4$(100) surface. Phys Rev Lett 107(3):036102

181. Rasmussen MK, Meinander K, Besenbacher F, Lauritsen JV (2012) Noncontact atomic force microscopy study of the spinel $MgAl_2O_4(111)$ surface. Beilstein J Nanotechnol 3:192–197
182. Kishimoto S, Kageshima M, Naitoh Y, Li YJ, Sugawara Y (2008) Study of oxidized Cu(110) surface using noncontact atomic force microscopy. Surf Sci 602(13):2175–2182
183. Lauritsen JV, Reichling M (2010) Atomic resolution non-contact atomic force microscopy of clean metal oxide surfaces. J Phys Condens Matter 22(26):263001
184. Irie H, Sunada K, Hashimoto K (2004) Recent developments in TiO_2 photocatalysis: novel applications to interior ecology materials and energy saving systems. Electrochemistry 72(12):807–812
185. Onishi H, Iwasawa Y (1994) Reconstruction of $TiO_2(110)$ surface – STM study with atomic-scale resolution. Surf Sci 313(1–2):L783–L789
186. Wendt S, Matthiesen J, Schaub R, Vestergaard EK, Laegsgaard E, Besenbacher F, Hammer B (2006) Formation and splitting of paired hydroxyl groups on reduced $TiO_2(110)$. Phys Rev Lett 96(6):066107
187. Schaub R, Thostrup P, Lopez N, Laegsgaard E, Stensgaard I, Norskov JK, Besenbacher F (2001) Oxygen vacancies as active sites for water dissociation on rutile TiO(2)(110). Phys Rev Lett 87(26):266104
188. Wendt S, Schaub R, Matthiesen J, Vestergaard EK, Wahlstrom E, Rasmussen MD, Thostrup P, Molina LM, Laegsgaard E, Stensgaard I, Hammer B, Besenbacher F (2005) Oxygen vacancies on $TiO_2(110)$ and their interaction with H_2O and O-2: a combined high-resolution STM and DFT study. Surf Sci 598(1–3):226–245
189. Foster AS, Pakarinen OH, Airaksinen JM, Gale JD, Nieminen RM (2003) Simulating atomic force microscopy imaging of the ideal and defected $TiO_2(110)$ surface. Phys Rev B 68(19):195410
190. Pinto HP, Enevoldsen GH, Besenbacher F, Lauritsen JV, Foster AS (2009) The role of tip size and orientation, tip-surface relaxations and surface impurities in simultaneous AFM and STM studies on the TiO(2)(110) surface. Nanotechnology 20(26):264020
191. Bammerlin M, Lüthi R, Meyer E, Baratoff A, Lü J, Guggisberg M, Gerber C, Howald L, Güntherodt HJ (1997) True atomic resolution on the surface of an insulator via ultrahigh vacuum dynamic force microscopy. Probe Microsc 1:3
192. Foster AS, Barth C, Shluger AL, Reichling M (2001) Unambiguous interpretation of atomically resolved force microscopy images of an insulator. Phys Rev Lett 86(11):2373–2376
193. Foster AS, Barth C, Shluger AL, Nieminen RM, Reichling M (2002) Role of tip structure and surface relaxation in atomic resolution dynamic force microscopy: $CaF_2(111)$ as a reference surface. Phys Rev B 66(23):235417
194. Barth C, Reichling M (2000) Resolving ions and vacancies at step edges on insulating surfaces. Surf Sci 470(1–2):L99–L103
195. Bennewitz R, Schar S, Barwich V, Pfeiffer O, Meyer E, Krok F, Such B, Kolodzej J, Szymonski M (2001) Atomic-resolution images of radiation damage in KBr. Surf Sci 474(1–3):L197–L202
196. Bennewitz R, Pfeiffer O, Schar S, Barwich V, Meyer E, Kantorovich LN (2002) Atomic corrugation in nc-AFM of alkali halides. Appl Surf Sci 188(3–4):232–237
197. Fujii S, Fujihira M (2007) Atomic contrast on a point defect on $CaF_2(111)$ imaged by non-contact atomic force microscopy. Nanotechnology 18(8):084011
198. Giessibl FJ, Reichling M (2005) Investigating atomic details of the $CaF_2(111)$ surface with a qPlus sensor. Nanotechnology 16(3):S118–S124
199. Hirth S, Ostendorf F, Reichling M (2006) Lateral manipulation of atomic size defects on the $CaF_2(111)$ surface. Nanotechnology 17(7):S148–S154
200. Hoffmann R, Lantz MA, Hug HJ, van Schendel PJA, Kappenberger P, Martin S, Baratoff A, Guntherodt HJ (2002) Atomic resolution imaging and force versus distance measurements on KBr(001) using low temperature scanning force microscopy. Appl Surf Sci 188(3–4):238–244

201. Bammerlin M, Luthi R, Meyer E, Baratoff A, Lu J, Guggisberg M, Loppacher C, Gerber C, Guntherodt HJ (1998) Dynamic SFM with true atomic resolution on alkali halide surfaces. Appl Phys Mater Sci Process 66:S293–S294
202. Barth C, Henry CR (2008) Imaging Suzuki precipitates on NaCl: Mg(2+)(001) by scanning force microscopy. Phys Rev Lett 100(9):096101
203. Barth C, Henry CR (2009) NaCl(001) surfaces nanostructured by Suzuki precipitates: a scanning force microscopy study. New J Phys 11(4):043003
204. Foster AS, Barth C, Henry CR (2009) Chemical identification of ions in doped NaCl by scanning force microscopy. Phys Rev Lett 102(25):256103
205. Bennewitz R, Foster AS, Kantorovich LN, Bammerlin M, Loppacher C, Schar S, Guggisberg M, Meyer E, Shluger AL (2000) Atomically resolved edges and kinks of NaCl islands on Cu(111): experiment and theory. Phys Rev B 62(3):2074–2084
206. Klust A, Ohta T, Bostwick AA, Yu QM, Ohuchi FS, Olmstead MA (2004) Atomically resolved imaging of a CaF bilayer on Si(111): subsurface atoms and the image contrast in scanning force microscopy. Phys Rev B 69(3):035405
207. Filleter T, Paul W, Bennewitz R (2008) Atomic structure and friction of ultrathin films of KBr on Cu(100). Phys Rev B 77(3):035430
208. Holscher H, Allers W, Schwarz UD, Schwarz A, Wiesendanger R (2000) Interpretation of "true atomic resolution" images of graphite (0001) in noncontact atomic force microscopy. Phys Rev B 62(11):6967–6970
209. Hembacher S, Giessibl FJ, Mannhart J, Quate CF (2003) Revealing the hidden atom in graphite by low-temperature atomic force microscopy. Proc Natl Acad Sci U S A 100(22):12539–12542
210. Kawai S, Kawakatsu H (2009) Surface-relaxation-induced giant corrugation on graphite (0001). Phys Rev B 79(11):115440
211. Ashino M, Schwarz A, Behnke T, Wiesendanger R (2004) Atomic-resolution dynamic force microscopy and spectroscopy of a single-walled carbon nanotube: characterization of interatomic van der Waals forces. Phys Rev Lett 93(13):136101
212. Loffler D, Uhlrich JJ, Baron M, Yang B, Yu X, Lichtenstein L, Heinke L, Buchner C, Heyde M, Shaikhutdinov S, Freund HJ, Wlodarczyk R, Sierka M, Sauer J (2010) Growth and structure of crystalline silica sheet on Ru(0001). Phys Rev Lett 105(14):146104
213. Lichtenstein L, Heyde M, Freund HJ (2012) Atomic arrangement in two-dimensional silica: from crystalline to vitreous structures. J Phys Chem C 116(38):20426–20432
214. Majzik Z, Tchalala MR, Svec M, Hapala P, Enriquez H, Kara A, Mayne AJ, Dujardin G, Jelinek P, Oughaddou H (2013) Combined AFM and STM measurements of a silicene sheet grown on the Ag(111) surface. J Phys Condens Matter 25(22):225301
215. Sun ZX, Hamalainen SK, Sainio J, Lahtinen J, Vanmaekelbergh D, Liljeroth P (2011) Topographic and electronic contrast of the graphene moire on Ir(111) probed by scanning tunneling microscopy and noncontact atomic force microscopy. Phys Rev B 83(8):081415
216. Boneschanscher MP, van der Lit J, Sun ZX, Swart I, Liljeroth P, Vanmaekelbergh D (2012) Quantitative atomic resolution force imaging on epitaxial graphene with reactive and nonreactive AFM probes. ACS Nano 6(11):10216–10221
217. Hamalainen SK, Boneschanscher MP, Jacobse PH, Swart I, Pussi K, Moritz W, Lahtinen J, Liljeroth P, Sainio J (2013) Structure and local variations of the graphene moire on Ir(111). Phys Rev B 88(20):6
218. Dedkov Y, Voloshina E (2014) Multichannel scanning probe microscopy and spectroscopy of graphene moire structures. Phys Chem Chem Phys 16(9):3894–3908
219. Fukui K, Onishi H, Iwasawa Y (1997) Imaging of individual formate ions adsorbed on TiO_2(110) surface by non-contact atomic force microscopy. Chem Phys Lett 280(3–4):296–301
220. Rahe P, Nimmrich M, Nefedov A, Naboka M, Woll C, Kuhnle A (2009) Transition of molecule orientation during adsorption of terephthalic acid on rutile TiO_2(110). J Phys Chem C 113(40):17471–17478

221. Schutte J, Bechstein R, Rahe P, Rohlfing M, Kuhnle A, Langhals H (2009) Imaging perylene derivatives on rutile TiO_2(110) by noncontact atomic force microscopy. Phys Rev B 79(4):045428
222. Loske F, Bechstein R, Schutte J, Ostendorf F, Reichling M, Kuhnle A (2009) Growth of ordered C_{60} islands on TiO_2(110). Nanotechnology 20(6):065606
223. Fremy S, Schwarz A, Lammle K, Prosenc M, Wiesendanger R (2009) The monomer-to-dimer transition and bimodal growth of Co-salen on NaCl(001): a high resolution atomic force microscopy study. Nanotechnology 20(40):405608
224. Lammle K, Trevethan T, Schwarz A, Watkins M, Shluger A, Wiesendanger R (2010) Unambiguous determination of the adsorption geometry of a metal-organic complex on a bulk insulator. Nano Lett 10(8):2965–2971
225. Pawlak R, Kawai S, Fremy S, Glatzel T, Meyer E (2011) Atomic-scale mechanical properties of orientated C(60) molecules revealed by noncontact atomic force microscopy. ACS Nano 5(8):6349–6354
226. Pawlak R, Kawai S, Fremy S, Glatzel T, Meyer E (2012) High-resolution imaging of C_{60} molecules using tuning-fork-based non-contact atomic force microscopy. J Phys Condens Matter 24(8):084005
227. Such B, Trevethan T, Glatzel T, Kawai S, Zimmerli L, Meyer E, Shluger AL, Amijs CHM, de Mendoza P, Echavarren AM (2010) Functionalized truxenes: adsorption and diffusion of single molecules on the KBr(001) surface. ACS Nano 4(6):3429–3439
228. Pawlak R, Fremy S, Kawai S, Glatzel T, Fang HJ, Fendt LA, Diederich F, Meyer E (2012) Directed rotations of single porphyrin molecules controlled by localized force spectroscopy. ACS Nano 6(7):6318–6324
229. Sasahara A, Uetsuka H, Onishi H (2001) NC-AFM topography of HCOO and CH(3)COO molecules co-adsorbed on TiO(2)(110). Appl Phys Mater Sci Process 72:S101–S103
230. Gritschneder S, Iwasawa Y, Reichling M (2007) Strong adhesion of water to CeO_2(111). Nanotechnology 18(4):044025
231. Burke SA, Mativetsky JM, Fostner S, Grutter P (2007) C_{60} on alkali halides: epitaxy and morphology studied by noncontact AFM. Phys Rev B 76(3):035419
232. Burke SA, Ledue JM, Topple JM, Fostner S, Grutter P (2009) Relating the functional properties of an organic semiconductor to molecular structure by nc-AFM. Adv Mater 21(20):2029–2033
233. Gotsmann B, Seidel C, Anczykowski B, Fuchs H (1999) Conservative and dissipative tip-sample interaction forces probed with dynamic AFM. Phys Rev B 60(15):11051–11061
234. Lantz MA, Hoffmann R, Foster AS, Baratoff A, Hug HJ, Hidber HR, Guntherodt HJ (2006) Site-specific force-distance characteristics on NaCl(001): measurements versus atomistic simulations. Phys Rev B 74(24):245426
235. Hoffmann R, Barth C, Foster AS, Shluger AL, Hug HJ, Guntherodt HJ, Nieminen RM, Reichling M (2005) Measuring site-specific cluster-surface bond formation. J Am Chem Soc 127(50):17863–17866
236. Hembacher S, Giessibl FJ, Mannhart J, Quate CF (2005) Local spectroscopy and atomic imaging of tunneling current, forces, and dissipation on graphite. Phys Rev Lett 94(5):056101
237. Albers BJ, Schwendemann TC, Baykara MZ, Pilet N, Liebmann M, Altman EI, Schwarz UD (2009) Data acquisition and analysis procedures for high-resolution atomic force microscopy in three dimensions. Nanotechnology 20(26):264002
238. Holscher H, Langkat SM, Schwarz A, Wiesendanger R (2002) Measurement of three-dimensional force fields with atomic resolution using dynamic force spectroscopy. Appl Phys Lett 81(23):4428–4430
239. Ashino M, Schwarz A, Holscher H, Schwarz UD, Wiesendanger R (2005) Interpretation of the atomic scale contrast obtained on graphite and single-walled carbon nanotubes in the dynamic mode of atomic force microscopy. Nanotechnology 16(3):S134–S137

240. Schwarz A, Holscher H, Langkat SM, Wiesendanger R (2003) Three-dimensional force field spectroscopy. AIP Conf Proc 696:68–78
241. Bhushan B (2002) Introduction to tribology. Wiley, New York
242. Bhushan B (2005) Nanotribology and nanomechanics: an introduction. Springer, Berlin
243. Giessibl FJ, Herz M, Mannhart J (2002) Friction traced to the single atom. Proc Natl Acad Sci U S A 99(19):12006–12010
244. Atabak M, Unverdi O, Ozer HO, Oral A (2009) Sub-Angstrom oscillation amplitude non-contact atomic force microscopy for lateral force gradient measurement. Appl Surf Sci 256(5):1299–1303
245. Weymouth AJ, Meuer D, Mutombo P, Wutscher T, Ondracek M, Jelinek P, Giessibl FJ (2013) Atomic structure affects the directional dependence of friction. Phys Rev Lett 111(12):126103
246. Kawai S, Glatzel T, Koch S, Such B, Baratoff A, Meyer E (2010) Ultrasensitive detection of lateral atomic-scale interactions on graphite (0001) via bimodal dynamic force measurements. Phys Rev B 81(8):085420
247. Ternes M, Lutz CP, Hirjibehedin CF, Giessibl FJ, Heinrich AJ (2008) The force needed to move an atom on a surface. Science 319(5866):1066–1069
248. Weymouth AJ, Hofmann T, Giessibl FJ (2013) Quantifying molecular stiffness and interaction with lateral force microscopy. Science 343:1120–1122
249. Welker J, Giessibl FJ (2012) Revealing the angular symmetry of chemical bonds by atomic force microscopy. Science 336(6080):444–449
250. Kimura K, Ido S, Oyabu N, Kobayashi K, Hirata Y, Imai T, Yamada H (2010) Visualizing water molecule distribution by atomic force microscopy. J Chem Phys 132(19):194705
251. Asakawa H, Yoshioka S, Nishimura K, Fukuma T (2012) Spatial distribution of lipid headgroups and water molecules at membrane/water interfaces visualized by three-dimensional scanning force microscopy. ACS Nano 6(10):9013–9020
252. Sugimoto Y, Jelinek P, Pou P, Abe M, Morita S, Perez R, Custance O (2007) Mechanism for room-temperature single-atom lateral manipulations on semiconductors using dynamic force microscopy. Phys Rev Lett 98(10):106104
253. Sugimoto Y, Pou P, Custance O, Jelinek P, Abe M, Perez R, Morita S (2008) Complex patterning by vertical interchange atom manipulation using atomic force microscopy. Science 322(5900):413–417